



**HAL**  
open science

# Experimental Constraints on Sulphur Behaviour in Subduction Zones: Implications for TTG and Adakite Production and the Global Sulphur Cycle since the Archean

Gaëlle Prouteau, Bruno Scaillet

► **To cite this version:**

Gaëlle Prouteau, Bruno Scaillet. Experimental Constraints on Sulphur Behaviour in Subduction Zones: Implications for TTG and Adakite Production and the Global Sulphur Cycle since the Archean. *Journal of Petrology*, 2013, 54 (1), pp.183-213. 10.1093/petrology/egs067 . insu-00757219

**HAL Id: insu-00757219**

**<https://insu.hal.science/insu-00757219v1>**

Submitted on 9 Dec 2016

**HAL** is a multi-disciplinary open access archive for the deposit and dissemination of scientific research documents, whether they are published or not. The documents may come from teaching and research institutions in France or abroad, or from public or private research centers.

L'archive ouverte pluridisciplinaire **HAL**, est destinée au dépôt et à la diffusion de documents scientifiques de niveau recherche, publiés ou non, émanant des établissements d'enseignement et de recherche français ou étrangers, des laboratoires publics ou privés.



Distributed under a Creative Commons Attribution - NonCommercial - NoDerivatives 4.0 International License

# Experimental Constraints on Sulphur Behaviour in Subduction Zones: Implications for TTG and Adakite Production and the Global Sulphur Cycle since the Archean

GAËLLE PROUTEAU<sup>1,2,3</sup> AND BRUNO SCAILLET<sup>1,2,3\*</sup>

<sup>1</sup>UNIVERSITE D'ORLÉANS, ISTO, UMR 7327, 45071, ORLÉANS, FRANCE

<sup>2</sup>CNRS/INSU, ISTO, UMR 7327, 45071 ORLÉANS, FRANCE

<sup>3</sup>BRGM, ISTO, UMR 7327, 45071 ORLÉANS, FRANCE

RECEIVED DECEMBER 10, 2010; ACCEPTED AUGUST 31, 2012  
ADVANCE ACCESS PUBLICATION OCTOBER 25, 2012

*We performed crystallization experiments at 2–3 GPa at 700–950°C on basaltic and pelitic lithologies with added water and sulphur to constrain the factors controlling sulphur behaviour in subduction zones and how it may have varied through geological time. The resulting hydrous silicic melts have up to 20 times more dissolved sulphur (up to 1 wt %) than at 0.2–0.4 GPa, when moderately oxidized conditions prevail. Such high solubilities appear to result from the combined effects of enhanced solubility of water in high-pressure silicate melts (10–20 wt % H<sub>2</sub>O), which acts to decrease silica activity, and oxidizing conditions. The results confirm previous findings that high sulphur contents in silicate melts do not necessarily require iron-rich compositions, suggesting instead that sulphur–water complexes play a fundamental role in sulphur dissolution mechanisms in iron-poor silicic melts, in agreement with recent spectroscopic data. The experimental melts reproduce Phanerozoic slab-derived magmas, in particular their distinct Ca- and Mg-rich composition. The results also show that sulphur increases the degree of melting of basalt lithologies. Hence, we suggest that subducted slabs will preferentially melt where sulphur is present in abundance and that the variability in arc magma sulphur output reflects, in part, the vagaries of sulphur distribution in the slab source. In contrast, comparison with the composition of Archean felsic rocks suggests that, in the early Earth, much less sulphur was present in subducted slabs, in agreement with a number of independent lines of evidence showing that the Archean ocean, hence the hydrothermally altered subducted Archean oceanic crust, was considerably poorer in*

*sulphur than at present. Volcanic degassing of sulphur was thus probably much weaker during the Archean than in Proterozoic–Phanerozoic times.*

KEY WORDS: adakite; magma; partial melting; sulphide; subduction; thermodynamics; igneous petrology; experimental petrology

## INTRODUCTION

The behaviour of sulphur in subduction zones remains largely unknown. A number of recent eruptions have illustrated that arc magmas are important contributors of sulphur to the atmosphere (Robock, 2000) with restored bulk sulphur contents prior to eruption (including those with a strong slab melt imprint) of *c.* 0.5 wt %, reaching several wt % in some instances (Scaillet *et al.*, 2003). Experiments and calculations have shown that most of the S is in the fluid phase (Scaillet *et al.*, 1998; Keppler, 1999; Burgisser & Scaillet, 2007; Burgisser *et al.*, 2008), which exsolves prior to eruption. High sulphur concentrations (up to 6000 ppm) in silicate-melt inclusions hosted in olivine from arc harzburgitic xenoliths and primitive basaltic lava samples (Métrich *et al.*, 1999; De Hoog *et al.*, 2001; Cervantes & Wallace, 2003) indicate that arc mantle may be significantly enriched in sulphur (up to 500 ppm)

relative to mid-ocean ridge basalt (MORB) mantle (*c.* 200 ppm), following metasomatism by an H<sub>2</sub>O-rich agent with up to several wt % sulphur (Cervantes & Wallace, 2003). Isotopic studies show that arc mantle sources are enriched in <sup>34</sup>S relative to MORB or ocean island basalt (OIB) sources (e.g.  $\delta^{34}\text{S}$  values between +4 and +7‰ for the Indonesian arc system; De Hoog *et al.*, 2001), pointing to the involvement of slab-derived material, in particular deep-sea sediments, which are on average significantly enriched in <sup>34</sup>S ( $\delta^{34}\text{S} = +12\%$ , Alt & Burdett, 1992), although other sources are possible [hydrothermally altered oceanic crust and serpentinized oceanic peridotites can have high sulphur contents, up to 1 wt % (Alt & Shanks, 2003)]. Recent high-pressure experiments have also shown that sulphate solubility is very high in Cl-bearing hydrous fluids (Newton & Manning, 2005). Similarly, experiments at 1.5 GPa on sulphides + H<sub>2</sub>O phase equilibria (Wykes & Mavrogenes, 2005) have shown that water depresses the melting temperature of sulphide, implying that molten sulphide can dissolve a significant amount of water. Thus, during dehydration at depth of serpentinite, which is the lithology believed to be the major source of fluids in subduction zones (Ulmer & Trommsdorff, 1995), sulphur is likely to be scavenged by percolating fluids, which will trigger melting in the upper sections of the downgoing slab. Recent thermodynamic modelling of sulphur behaviour in metamorphosed continental crust has shown that this element is easily remobilized by pervading metamorphic fluids (Tomkins, 2010). This scenario is also likely to be valid for oceanic crust at the deeper conditions imposed by subduction. In addition to hydrothermally altered basaltic or ultramafic crust, widespread sulphide accumulation deposits occurring on the seafloor [the so-called volcanic-hosted massive sulphide deposits (VHMS); see Huston *et al.* (2010) for a review] are another, immediately available, source of sulphur, with concentrations largely exceeding the wt % level, which, if subducted, may also be remobilized. All the evidence points, therefore, to efficient mass transfer of sulphur in the subduction factory. However, although massive subduction recycling of sulphur has been advocated for Phanerozoic times (e.g. Jambon, 1994), whether this was also the case during the Archean is not known.

Slab-derived melts are generally not considered as the main transport medium of sulphur (e.g. De Hoog *et al.*, 2001) because (1) this requires sulphur concentrations of at least 10 000 ppm, which exceeds by 2–3 orders of magnitude the known solubility of sulphur in common siliceous melts at low pressures, and (2) geothermal gradients in present-day subduction zones have been long considered too cold to allow widespread slab melting, except under restricted conditions (subduction of young hot slabs). The second limitation is now challenged by the fact that improved thermal models with temperature-dependent

and/or stress-dependent rheology (e.g. van Keken *et al.*, 2002; Kelemen *et al.*, 2003), point to top slab temperatures high enough to allow fluid-saturated melting of the subducted slab. In support of this are recent findings based on trace element solubilities in high-pressure fluids and melts that point to the temperatures at the top of the slab high enough to allow its melting (i.e. >700°C; Plank *et al.*, 2009). Additionally, sediment partial melting is required for critical elements such as Th and Be to be efficiently transferred into the mantle wedge (Johnson & Plank, 1999; Hermann & Spandler, 2008), which calls for partial melting of subducted slabs to be more common than generally thought. With respect to the first limitation, no experimental study has yet explored the solubility of sulphur in hydrous silicic melt at high pressures. Available experimental constraints on sulphur solubility in silicate melts at high pressures concern mostly dry basaltic compositions (e.g. Wendlandt, 1982; Mavrogenes & O'Neill, 1999; Holzeid & Grove, 2002; Jugo *et al.*, 2005), which are not appropriate to most subduction zone environments.

Within this context we have investigated the sulphur solubility in melts produced from partial melting of basalt and sediment, under  $P$ – $T$ – $f\text{O}_2$  conditions relevant to subduction zones. Our approach consisted of adding sulphur to basalt–H<sub>2</sub>O or sediment–H<sub>2</sub>O charges, whose melting behaviour without sulphur had been previously determined (Prouteau *et al.*, 2001; Hermann & Spandler, 2008). We explored the effect of oxygen fugacity ( $f\text{O}_2$ ), owing to its influence on sulphur behaviour in silicate melts (Carroll & Rutherford, 1987; Luhr, 1990; Carroll & Webster, 1994; Scaillet & Evans, 1999; O'Neill & Mavrogenes, 2002; Jugo *et al.*, 2005), from around NNO +1 (one log unit above the solid buffer nickel–nickel oxide) to below NNO – 2. We explored a range of 1–4 wt % bulk sulphur content to determine the maximum sulphur content in silicate melts under these conditions. It should be noted that we do not argue that the oceanic crust is everywhere enriched at the per cent level in sulphur, but rather that such concentrations may locally be reached and exert a first-order control on the observed variability in the sulphur output of arc magmas (e.g. Scaillet *et al.*, 2003). We investigated a pressure and temperature range of 2–3 GPa and 700–950°C, respectively. Such conditions include those of the top of the subducted slab beneath the majority of active volcanic arcs and are thus supposed to mimic slab melting (Defant & Drummond, 1990; Schmidt & Poli, 1998; Kelemen *et al.*, 2003; Hermann & Spandler, 2008). We have not explored higher pressures primarily to avoid approaching too closely the second critical end point (Bureau & Keppler, 1999; Kessel *et al.*, 2005a, 2005b; Klimm *et al.*, 2008), which for the basalt–H<sub>2</sub>O system is considered to lie between 5 and 6 GPa (Kessel *et al.* 2005b). The experimental pressures are thus sufficiently high to approach slab melting conditions, but also low enough to avoid H<sub>2</sub>O contents of

the experimental melts too high to render them unquenchable (Klimm *et al.*, 2008). Our results are then applied to the broad context of oceanic subduction, past to recent, in an effort to unravel the role of silicate melts produced in such an environment on the global cycle of sulphur.

## EXPERIMENTAL AND ANALYTICAL PROCEDURES

### Apparatus and starting material

Experiments were performed at 2–3 GPa and between 700 and 950°C on a representative MORB from the Juan de Fuca Ridge (Prouteau *et al.*, 2001) and a pelitic sediment from the Barbados accretionary prism, Lesser Antilles (Table 1). Experiments were conducted in a ½ inch piston-cylinder apparatus using talc–Pyrex–graphite furnace assemblies. We used gold capsules (outer diameter 1.8 mm; inner diameter 1.6 mm; length 10 mm) packed within the graphite furnace with boron nitride powder. The use of these assemblies and gold capsules produces  $fO_2$  conditions around the Ni–NiO transition (see below). Capsules were separated from the thermocouple by a 1 mm thick MgO wafer. Temperature was controlled using

an S-type thermocouple sitting 1 mm above the capsule. No friction correction was applied and nominal pressures are reported. Run durations were between 1 and 5 days (Table 2), depending on temperature.

Basalt experiments were performed using the same dry glass as in the study by Prouteau *et al.* (2001) as the starting product, prepared by fusing twice at 0.001 MPa a powdered MORB. We added 5.5–8.0 wt % H<sub>2</sub>O [following Prouteau *et al.* (2001)], and 1–2 wt % elemental sulphur to the MORB experimental charges. In one experiment with basalt (charge MS11), reducing conditions were achieved by using a graphite capsule lining a platinum capsule, within which the starting glass powder and water were loaded. The use of a graphite capsule buffers the redox conditions at *c.* 2 log units below NNO (see below).

The pelite has an initial mineralogy of mainly quartz and clay (smectite, kaolinite, illite). We conducted the experiments directly using the powdered pelite, which has ~8.5 wt % H<sub>2</sub>O bound in hydrous minerals, with 1–4 wt % added elemental sulphur.

The use of elemental sulphur as a source of sulphur, instead of pyrrhotite or anhydrite as commonly practised (e.g. Luhr, 1990; Jugo *et al.*, 2010), needs discussion. We are interested in a process whereby sulphur is brought to the system via the ingress of hydrous fluids (i.e. those released by dewatering of altered oceanic crust). The tested hypothesis is that those hydrous fluids may contain several wt % dissolved S. Using either pyrrhotite or anhydrite as a source of S would imply that slab-derived fluids contain S and Fe (or Ca) in equal proportions, an unjustified assumption, which would also introduce an additional compositional bias in the system. In fact, our procedure is similar to that of adding water or any other volatile whose effect on phase relations or compositions is being considered: introduction of water allows crystallization of hydrous phases, whereas introduction of CO<sub>2</sub> allows carbonate precipitation. Hence, we believe that our experimental procedure more closely simulates what can happen at depth in crustal sections flushed by S-bearing fluids than one in which sulphur is added either as FeS or as CaSO<sub>4</sub>. It is clear, however, that our experiments still do not fully simulate the real system: in particular, the role of halogens (Cl, F) should be explored in future studies.

A last note concerns the presence of CO<sub>2</sub> in the pelite charges (1 wt % in the starting material; Table 1). The presence of this volatile should increase the potential for fluid saturation of pelite-based experiments, yet this is difficult to assess owing to the fact that CO<sub>2</sub> solubility trends in high-pressure hydrous silicic melts are poorly known. Although there is no evidence, either textural (i.e. large bubbles) or on capsule opening (hissing), for the coexistence of a separate fluid phase with the silicate melt during the HP–HT annealing, we cannot fully exclude such a possibility. In any case, it should be kept in mind that the

Table 1: Starting compositions

|                                 | Pelite<br>B-12a | Pelite<br>B-12a<br>Anhydrous | N-MORB<br>BN06-11<br>Anhydrous |
|---------------------------------|-----------------|------------------------------|--------------------------------|
| SiO <sub>2</sub>                | 58.49           | 64.80                        | 49.97                          |
| TiO <sub>2</sub>                | 0.87            | 0.97                         | 2.27                           |
| Al <sub>2</sub> O <sub>3</sub>  | 19.35           | 21.43                        | 13.68                          |
| FeO <sub>tot</sub>              | 5.59            | 6.19                         | 12.69                          |
| FeO                             | 1.67            | -                            | -                              |
| MnO                             | 0.04            | 0.04                         | 0.22                           |
| MgO                             | 1.95            | 2.16                         | 6.83                           |
| CaO                             | 0.36            | 0.40                         | 10.56                          |
| Na <sub>2</sub> O               | 1.31            | 1.46                         | 2.69                           |
| K <sub>2</sub> O                | 2.21            | 2.45                         | 0.27                           |
| P <sub>2</sub> O <sub>5</sub>   | 0.09            | 0.10                         | 0.37                           |
| LOI                             | 8.53            | -                            | -                              |
| Total                           | 100.46          | 100.00                       | 99.54                          |
| CO <sub>2</sub> tot %           | 1.03            | -                            | -                              |
| H <sub>2</sub> O tot %          | 8.53            | -                            | -                              |
| H <sub>2</sub> O <sup>-</sup> % | 2.53            | -                            | -                              |
| S tot %                         | 0.090           | -                            | -                              |
| Cl ppm                          | 565             | -                            | -                              |
| F %                             | 0.056           | -                            | -                              |

LOI, loss on ignition.

Table 2: *Experimental conditions and run products*

| Run no.       | $P$ (GPa) | $T$ (°C) | $fO_2$ | Duration (h) | H <sub>2</sub> O (wt %) | S bulk (wt %) | Run products                          | S melt (ppm) | $n$ |
|---------------|-----------|----------|--------|--------------|-------------------------|---------------|---------------------------------------|--------------|-----|
| <i>Basalt</i> |           |          |        |              |                         |               |                                       |              |     |
| MS7           | 2         | 800      | +1     | 66           | 6.7                     | 1.1           | Gl, Hbl, Tmg, Anh                     | 290(22)      | 7   |
| MS6           | 2         | 900      | +1     | 41           | 6.6                     | 1.1           | Gl, Hbl, Hilm, Po                     | 300(56)      | 11  |
| MS26          | 2         | 900      | +1     | 48           | 6.0                     | 2.0           | Gl, Hbl, Hilm, Po                     | 1509(94)     | 12  |
| MS29          | 2         | 950      | +1     | 40           | 6.5                     | 2.0           | Gl, Hbl, Cpx, Opx, Tmg, Hilm, Anh, Po | 1912(620)    | 19  |
| MS5           | 3         | 800      | +1     | 65           | 6.2                     | 1.1           | Gl, Ga, Cpx, Rut, Ap, Po              | 93(29)       | 9   |
| MS1           | 3         | 900      | +1     | 42           | 5.4                     | 1.1           | Gl, Ga, Cpx, Rut, Po                  | 1260(113)    | 7   |
| MS22          | 3         | 700      | +1     | 75           | 6.8                     | 2.0           | Gl, Hbl, Ep, Hilm, Rut, Coe, Anh      | 570(29)      | 4   |
| MS10          | 3         | 800      | +1     | 67           | 6.6                     | 2.0           | Gl, Ga, Cpx, Hbl, Rut, Anh, Po        | 1284(95)     | 8   |
| MS9           | 3         | 900      | +1     | 43           | 5.4                     | 2.0           | Gl, Ga, Cpx, Rut, Anh, Po             | 4592(377)    | 15  |
| MS11          | 3         | 900      | <-2    | 50           | 8.1                     | 2.0           | Gl, Ga, Cpx, Rut, Po                  | 228(28)      | 9   |
| MS24          | 3         | 950      | +1     | 21           | 7.3                     | 2.0           | Gl, Ga, Cpx, Opx, Rut, Hilm, Anh, Po  | 5031(427)    | 18  |
| <i>Pelite</i> |           |          |        |              |                         |               |                                       |              |     |
| PEL1          | 3         | 900      | +1     | 89           | 8.5                     | 1.0           | Gl, Ga, Al Sil, Rut, Po               | 251(31)      | 6   |
| PEL2          | 3         | 900      | +1     | 73           | 8.5                     | 4.0           | Gl, Al Sil, Opx, Rut, Po              | 9768(152)    | 14  |
| PEL3          | 3         | 800      | +1     | 91           | 8.5                     | 4.0           | Gl, Al Sil, Opx, Phlog, Coe, Rut, Po  | 2540(81)     | 11  |

$fO_2$  is given in log units relative to NNO. Approximate values are indicated only. (See text for explanation.)  $n$  corresponds to the number of analyses of sulphur. Numbers in parentheses correspond to the standard deviation ( $1\sigma$ ). For basaltic charges, the amount of H<sub>2</sub>O is that loaded to the capsule together with the dry glass. For pelitic charges, the amount of water corresponds to that of sample, as listed in Table 1. Gl, glass; Hbl, hornblende; Cpx, clinopyroxene; Opx, orthopyroxene; Ga, garnet; Phlog, phlogopite; Al Sil, aluminium silicate; Coe, coesite; Ep, epidote; Tmg, titanomagnetite; Hilm, hemoilmenite; Rut, rutile; Anh, anhydrite; Po, pyrrhotite.

geochemical inferences derived below from pelite experiments correspond to a pelite composition with a significant amount of CO<sub>2</sub>.

### Analytical techniques

Upon run completion, capsules were recovered and cut in half. Half of each capsule + run products was mounted in epoxy resin, and polished for scanning electron microscopy (SEM) and electron microprobe (EMP) analyses [Cameca SX 50 (Services Communs BRGM–CNRS–Université d’Orléans, Orléans) and Cameca SX 100 (Services Communs Camparis, Paris)].

Major elements of both glasses and crystals were determined with the following analytical conditions: accelerating voltage of 15 kV, sample current of 6 nA, counting time of 10 s on peak, with either a defocused (glass, 10–15  $\mu$ m) or focused (crystal) beam. The measured alkali concentrations of the glasses were corrected by using secondary standards of rhyolitic composition with known alkali and water contents (Scaillet *et al.*, 1995). The water contents of the experimental glasses were determined by using the summation deficit from 100% of the EMP analyses (Devine *et al.*, 1995), using eight rhyolitic standard glasses containing 2–8.7 wt % H<sub>2</sub>O as determined by Karl Fisher titration (Martel *et al.*, 1998; Scaillet & Evans,

1999) or ion-microprobe analysis (Scaillet *et al.*, 1995). Owing to potential volatile exsolution during quench, we also calculated the amount of dissolved H<sub>2</sub>O on the basis of perfectly incompatible behaviour of K<sub>2</sub>O and H<sub>2</sub>O in experimental runs where no hydrous and/or potassic phases are left in the residue.

After having determined their major element composition, the sulphur content of the glasses was determined using the following analytical conditions: accelerating voltage of 15 kV, sample current of 50 nA, counting time of 180 s and a focused beam, which ensure a detection limit of 50 ppm. We used three S-bearing glass standards whose sulphur contents have been determined by wet chemistry (Clemente *et al.*, 2004). No attempt was made to determine the sulphur speciation through the peak-shift method (Carroll & Rutherford, 1988). However, the occurrence of anhydrite in several of our charges suggests that significant sulphate is present (Carroll & Rutherford, 1988).

### Redox state of the experiments

It is well known that controlling  $fO_2$  in solid-medium pressure devices used to simulate mantle conditions is a hard task (Holloway *et al.*, 1992; Rosenbaum & Slagel, 1995; Brooker *et al.*, 1998; Hall *et al.*, 2004). Unlike in gas pressure vessels, where  $fH_2$  (hydrogen fugacity)/ $fO_2$  can be strictly

controlled via  $H_2$ -Ar mixtures (e.g. Scaillet *et al.*, 1992), in piston cylinder apparatus, the  $fO_2$  is considered to be largely imposed by the solid-medium assembly. The type of assembly we used (talc-Pyrex-graphite furnace) has been shown to impose relatively oxidizing conditions in hydrous charges, around NNO (Patiño Douce & Beard, 1994; Trukenbrodt *et al.*, 1997; Ratajeski & Sisson, 1999; Pichavant *et al.*, 2002). For instance, in a phase equilibrium study performed on hydrous arc basalts, Pichavant *et al.* (2002) used the spinel-olivine-liquid equilibrium to show that the  $fO_2$  of charges varies from NNO + 0.6 up to NNO + 2.8. This corresponds to an intrinsic  $fH_2$  around 20–40 bar in the investigated  $P$ - $T$  range (see below). Our charges have dissolved  $H_2O$  contents mostly in the range 10–20 wt % (see results), and such a range of variation in  $fH_2O$  (water fugacity) induces in turn a range of  $fO_2$  (Whitney, 1972; Webster *et al.*, 1987; Scaillet *et al.*, 1995). To illustrate this, Fig. 1 shows the results of  $fO_2$  variations arising from different  $fH_2O$  at 3 GPa and for two temperatures, 700 and 900 °C (note that the relationships shown hold true regardless of the presence or absence of a separate fluid phase). We have assumed that, at 900 °C, a

melt with 15 wt % dissolved  $H_2O$  is at NNO + 1, which gives an  $fH_2$  of 40 bar [using the model of Zhang (1999) to calculate  $fH_2O$  from dissolved  $H_2O$  contents at  $P$  and  $T$ ]. Under those conditions, a charge with a melt water content of 10 wt % will have an intrinsic  $fO_2$  at NNO + 0.5, whereas one with 20 wt % dissolved  $H_2O$  will be at NNO + 1.5. Decreasing temperature to 700 °C would increase the corresponding  $fO_2$ . Therefore, variations in melt  $H_2O$  content induce changes in  $fO_2$ , which remains within 0.5 log unit of the average value. Drastic changes in  $fO_2$  will occur only in very water-poor melts; that is, melts with dissolved water contents much lower than 5 wt % (Fig. 1).

The occurrence of anhydrite in several charges (see below) is taken as further evidence for the success of the talc-Pyrex assembly in promoting rather oxidizing conditions. Several studies performed at lower pressures have shown that anhydrite crystallizes only when  $fO_2$  is higher than NNO, more probably above NNO + 1 (Carroll & Rutherford, 1987, 1988; Luhr, 1990; Carroll & Webster, 1994; Scaillet & Evans, 1999; Clemente *et al.*, 2004; Costa *et al.*, 2004; Jugo *et al.*, 2005; Scaillet & Macdonald, 2006;

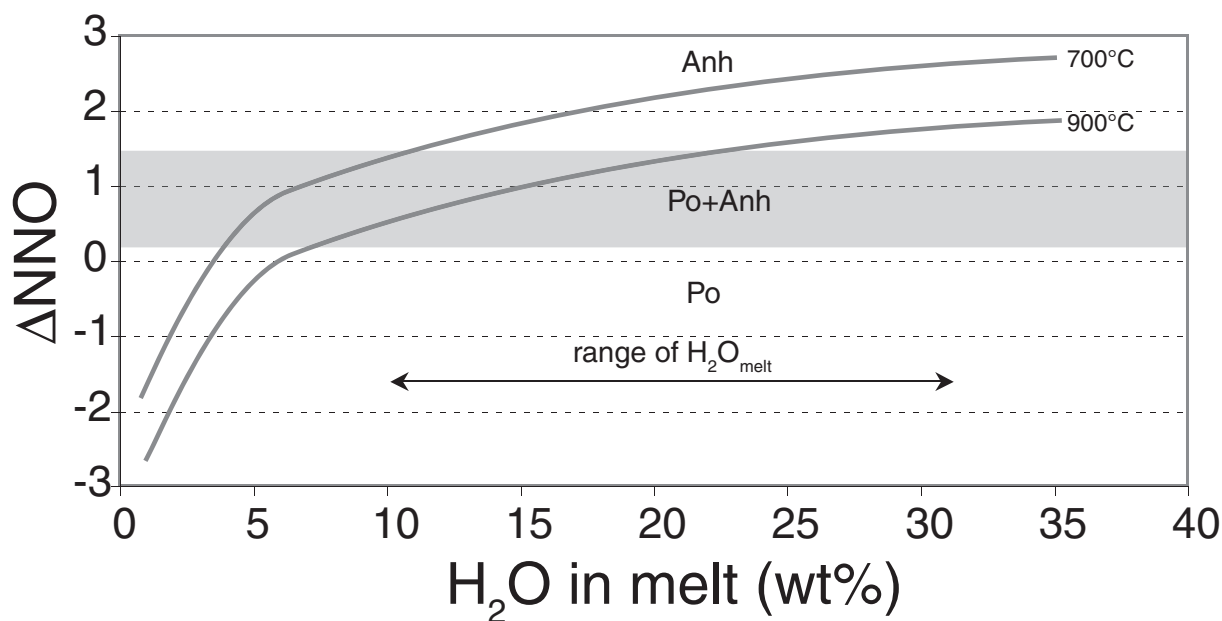


**Fig. 1.** Effect of  $H_2O$  dissolved in the melt on the  $fO_2$  imposed on the charge, calculated at 3 GPa for two temperatures using an intrinsic  $fH_2$  of 4 MPa, assumed to be fixed by the piston cell assembly. Variations of melt water contents in the range 10–30 wt % produce only slight variations in  $fO_2$ . It is only when the  $H_2O$  content is below 5 wt % that an exponential decrease in  $fO_2$  arises. Also shown are the fields of pyrrhotite (Po) and anhydrite (Anh) stability as determined in low-pressure, low-temperature experiments (Luhr, 1990; Carroll & Webster, 1994; Scaillet *et al.*, 1998; Clemente *et al.*, 2004; Scaillet & Macdonald, 2006), together with the  $fO_2$  domain where they coexist (shaded area). It should be noted that, relative to a charge in which both anhydrite and pyrrhotite coexist, a charge having a lower content of dissolved  $H_2O$  may precipitate only pyrrhotite, whereas one with higher  $H_2O$  will crystallize only anhydrite. Similarly, for the same  $P$ , dissolved  $H_2O$  and bulk S content (taken as a proxy of  $fS_2$ ), a low-temperature run will impose a slightly higher  $fO_2$  on the charge relative to that performed at high temperature [compare charges MS7 (800 °C) and MS6 (900 °C)]. At any given  $P$ , for a same piston cell assembly, changes in the S-bearing solid phases may arise from the combined effects of temperature,  $fH_2O$  (change in melt  $H_2O$  content) and  $fS_2$  (different bulk S content). Horizontal arrow shows the range of  $H_2O$  in the melt inferred from mass balancing  $K_2O$  and  $H_2O$ , assuming incompatible behaviour for both components.

Parat *et al.*, 2008), and the  $f\text{O}_2$  range over which both sulphide and sulphate coexist, as in some of our charges, is narrow, of the order of 0.5 log units or so (e.g. Scaillet *et al.*, 1998; Jugo *et al.*, 2010). Thermodynamic considerations on sulphide and sulphate stabilities in the Fe–Si–S–O–Ca–Ti–H system also show that this occurs at around NNO + 1 (Luhr, 1990). The implication is that a small departure in  $f\text{O}_2$  resulting from variations in  $f\text{H}_2\text{O}$  may drive the system outside the  $f\text{O}_2$  range of co-stability, toward either the anhydrite-only or the sulphide-only field, as illustrated in Fig. 1. We thus suggest that the lack of anhydrite in some charges is in part due to this effect, in addition to changes related to small variations in intrinsic  $f\text{H}_2$  and/or variations in  $f\text{S}_2$  [caused by varying bulk amounts of sulphur; see Clemente *et al.* (2004) and below]. Based on the above lines of evidence we conclude that the average imposed  $f\text{O}_2$  in our oxidized experiments was around NNO + 1.

For the graphite-lined capsule (charge MS11, Tables 2 and 3), various studies have shown that such an assembly imposes fairly reduced conditions (Holloway *et al.*, 1992). Ulmer & Luth (1991) have shown that when  $f\text{H}_2$  is buffered by the hematite–magnetite solid outer assembly the corresponding  $f\text{O}_2$  inside a capsule lined with graphite and equilibrated with a C–O–H fluid is close to NNO (at 3 GPa and 900°C). According to the evidence presented above (Fig. 1), we estimate that the  $f\text{H}_2$  imposed by our piston cylinder assembly is *c.* 30–40 bars in the investigated  $P$ – $T$  range, which should allow a maximum  $f\text{O}_2$  of around NNO – 2 (i.e. graphite-saturated conditions and a C–O–H fluid). It should be noted that the procedure used implies that C-bearing species are present in the reduced basaltic charge.

## Calculation of $f\text{S}_2$

The small size of sulphide phases prevents their accurate chemical characterization and thus the determination of  $f\text{S}_2$  via their composition (Clemente *et al.*, 2004). In our study we have evaluated the prevailing  $f\text{S}_2$  by applying the method of Bockrath *et al.* (2004), as modified by Liu *et al.* (2007). Those workers have derived a simple empirical expression that allows calculation of the  $f\text{S}_2$  of a silicate liquid saturated in sulphide liquid. The master equation is



Although originally designed and calibrated on basaltic compositions and within the temperature range 1200–1400°C, Liu *et al.* (2007) have shown that the empirical expression of Bockrath *et al.* (2004) recovers measured  $f\text{S}_2$  of hydrous and low-temperature melts to within 0.7 log unit. The expression is

$$\log f\text{S}_2 = 6.7 - 12800/T - 2\log X_{\text{FeO}} + \Delta\text{FMQ} + 0.904(P - 1)/2 \cdot 303RT \quad (2)$$

where  $T$  is in K,  $P$  in bar,  $X_{\text{FeO}}$  is the mole fraction of FeO in the melt,  $\Delta\text{FMQ}$  the  $f\text{O}_2$  expressed relative to the fayalite–quartz–magnetite solid buffer [note that a similar result would be obtained with the expression derived by O'Neill & Mavrogenes (2002) but for purposes of comparison with Liu *et al.* (2007) we use the modified Bockrath *et al.* (2004) equation]. Application of such an equation to our melts yields  $\log f\text{S}_2$  ranging from –1 to over 5, most charges having  $\log f\text{S}_2$  in the range 2–4 (Fig. 2, Table 3), the higher value being attained in the oxidized and sulphur-rich charges. Despite some scatter, a broad positive correlation is observed between  $f\text{S}_2$  and sulphur content of the melt [excluding the charges MS5 and PEL1, which fall clearly outside the main trend (Fig. 2)]. A linear regression through the remaining dataset yields a correlation coefficient  $r^2 = 0.7$ . Such a trend reflects the general increase in sulphur fugacity that is produced by adding more sulphur to the charge. Although approximate, the elevated  $f\text{S}_2$  calculated for our charges can be understood in the following way. Let us consider a silicate melt saturated in sulphide at a given  $f\text{O}_2$ . The equilibrium constant of reaction (1) is

$$K = f\text{O}_2(a_{\text{FeS}})^2 / f\text{S}_2(a_{\text{FeO}})^2 \quad (3)$$

where  $a_{\text{FeS}}$  and  $a_{\text{FeO}}$  stand for the activity of either melt or solid components FeS and FeO. At fixed  $f\text{O}_2$ , owing to the restricted range of sulphide composition, variations in  $a_{\text{FeO}}$  (thus FeO content) must be largely compensated by that of  $f\text{S}_2$  to maintain equilibrium. A variation in FeO from 10 wt % (basalt) down to 1 wt % (rhyolite) induces a decrease in  $X_{\text{FeO}}$  by an order of magnitude. Because the activity of ferrous oxide in anhydrous or hydrous silicate melts is not far from unity (Gaillard *et al.*, 2003) this implies a similar decrease in  $a_{\text{FeO}}$ . Assuming ideal behaviour and  $a_{\text{FeS}} = 1$ , it can be easily calculated from equation (3) that, for a change in  $X_{\text{FeO}}$  from 0.1 to 0.01, the corresponding increase in  $f\text{S}_2$  is two orders of magnitude to maintain sulphide saturation and four orders of magnitude if  $X_{\text{FeO}}$  goes down to 0.001. Most of our melts have  $X_{\text{FeO}}$  in the range 0.01–0.001. This thus explains the very large difference observed between  $f\text{S}_2$  of basaltic melts saturated in sulphide (Wallace & Carmichael, 1992; O'Neill & Mavrogenes, 2002; Liu *et al.*, 2007; Moune *et al.*, 2009) when compared with silicic melts saturated in sulphide.

## EXPERIMENTAL RESULTS

### Run products

#### General

Details of the experimental conditions and run products are listed in Table 2 and illustrated in Fig. 3. Within error, no systematic variations in most mineral or melt compositions were found across the length of the experimental charges. Limited mineral zoning was found only in garnet

Table 3: Experimental garnet compositions

| Run no.:  | MS5   |       |       |       | MS1   |       |       |       | MS10  |       |       |       | MS9   |       |       |       |
|---|-------|-------|-------|-------|-------|-------|-------|-------|-------|-------|-------|-------|-------|-------|-------|-------|
| P (GPa):  | 3     |       |       |       | 3     |       |       |       | 3     |       |       |       | 3     |       |       |       |
| T (°C):   | 800   |       |       |       | 900   |       |       |       | 800   |       |       |       | 900   |       |       |       |
| H <sub>2</sub> O (wt %):                        | 6.2   |       |       |       | 5.4   |       |       |       | 6.6   |       |       |       | 5.4   |       |       |       |
| S (wt %):                                       | 1.1   |       |       |       | 1.1   |       |       |       | 2     |       |       |       | 2     |       |       |       |
|   | Core  |       | Rim   |       | Core  |       | Rim   |       | Core  |       | Rim   |       | Core  |       | Rim   |       |
| Analyses:                                       | 6     | SD    | 7     | SD    | 5     | SD    | 6     | SD    | 7     | SD    | 9     | SD    | 6     | SD    | 6     | SD    |
| <i>wt % oxide</i>                               |       |       |       |       |       |       |       |       |       |       |       |       |       |       |       |       |
| SiO <sub>2</sub>                                | 37.14 | 0.29  | 37.84 | 0.58  | 38.04 | 0.56  | 38    | 0.69  | 37.9  | 0.45  | 38.23 | 0.54  | 38.34 | 0.45  | 38.56 | 0.56  |
| TiO <sub>2</sub>                                | 2.09  | 0.05  | 1.26  | 0.16  | 1.95  | 0.24  | 1     | 0.19  | 1.21  | 0.1   | 1.3   | 0.45  | 1.66  | 0.25  | 1.05  | 0.04  |
| Al <sub>2</sub> O <sub>3</sub>                  | 19.03 | 0.19  | 20.01 | 0.29  | 18.9  | 0.21  | 19.51 | 0.36  | 20.22 | 0.35  | 20.21 | 0.82  | 19.33 | 0.18  | 19.86 | 0.34  |
| FeO   | 21.84 | 0.48  | 21.02 | 0.31  | 20.52 | 0.23  | 19.92 | 0.47  | 20.94 | 0.96  | 20.38 | 0.39  | 19.94 | 0.58  | 19.44 | 0.36  |
| MnO   | 0.64  | 0.16  | 0.4   | 0.04  | 0.61  | 0.12  | 0.49  | 0.04  | 1.36  | 0.35  | 0.84  | 0.17  | 0.61  | 0.08  | 0.55  | 0.07  |
| MgO   | 6.56  | 0.54  | 7.99  | 0.31  | 9.56  | 0.34  | 8.57  | 0.23  | 6.25  | 0.36  | 7.26  | 0.25  | 10.15 | 0.56  | 9.9   | 0.59  |
| CaO   | 10.02 | 0.31  | 8.79  | 0.33  | 8.38  | 0.25  | 9.64  | 0.22  | 11    | 0.57  | 10.54 | 0.72  | 8.13  | 0.38  | 8.88  | 0.34  |
| Na <sub>2</sub> O                               | 0.07  | 0.03  | 0.12  | 0.04  | 0.09  | 0.02  | 0.1   | 0.05  | 0.08  | 0.05  | 0.08  | 0.06  | 0.07  | 0.03  | 0.1   | 0.02  |
| Total   | 97.39 | 0.56  | 97.43 | 1.3   | 98.04 | 0.97  | 97.23 | 0.77  | 98.98 | 0.83  | 98.84 | 0.43  | 98.24 | 0.47  | 98.33 | 0.75  |
| <i>Structural formula (based on 12 oxygens)</i> |       |       |       |       |       |       |       |       |       |       |       |       |       |       |       |       |
| Si  | 2.962 | 0.019 | 2.981 | 0.01  | 2.975 | 0.015 | 2.994 | 0.028 | 2.968 | 0.022 | 2.977 | 0.032 | 2.979 | 0.021 | 2.987 | 0.021 |
| Ti  | 0.125 | 0.004 | 0.074 | 0.009 | 0.115 | 0.013 | 0.06  | 0.011 | 0.071 | 0.006 | 0.076 | 0.027 | 0.097 | 0.015 | 0.061 | 0.003 |
| Al <sub>tot</sub>                               | 1.789 | 0.012 | 1.859 | 0.011 | 1.742 | 0.007 | 1.812 | 0.018 | 1.867 | 0.036 | 1.855 | 0.07  | 1.77  | 0.02  | 1.813 | 0.019 |
| Fe <sub>tot</sub>                               | 1.457 | 0.036 | 1.385 | 0.024 | 1.342 | 0.026 | 1.313 | 0.037 | 1.371 | 0.059 | 1.327 | 0.025 | 1.296 | 0.041 | 1.26  | 0.031 |
| Mn  | 0.043 | 0.011 | 0.027 | 0.003 | 0.04  | 0.008 | 0.033 | 0.003 | 0.091 | 0.023 | 0.055 | 0.011 | 0.04  | 0.005 | 0.036 | 0.005 |
| Mg  | 0.78  | 0.06  | 0.938 | 0.024 | 1.114 | 0.028 | 1.006 | 0.035 | 0.73  | 0.041 | 0.842 | 0.025 | 1.175 | 0.061 | 1.144 | 0.064 |
| Ca  | 0.856 | 0.03  | 0.742 | 0.03  | 0.702 | 0.027 | 0.814 | 0.019 | 0.923 | 0.047 | 0.879 | 0.063 | 0.677 | 0.03  | 0.737 | 0.031 |
| Na  | 0.012 | 0.004 | 0.018 | 0.005 | 0.014 | 0.003 | 0.016 | 0.007 | 0.013 | 0.007 | 0.013 | 0.008 | 0.011 | 0.005 | 0.015 | 0.004 |
| Total   | 8.024 |       | 8.024 |       | 8.045 |       | 8.048 |       | 8.034 |       | 8.025 |       | 8.044 |       | 8.053 |       |
| Mg#   | 0.35  | 0.02  | 0.4   | 0.01  | 0.45  | 0.01  | 0.43  | 0.01  | 0.35  | 0.02  | 0.39  | 0.01  | 0.48  | 0.02  | 0.48  | 0.02  |
| Spessartine                                     | 1.4   | 0.3   | 0.9   | 0.1   | 1.3   | 0.3   | 1     | 0.1   | 2.9   | 0.8   | 1.8   | 0.4   | 1.3   | 0.2   | 1.1   | 0.1   |
| Almandine                                       | 42.1  | 1.4   | 41.8  | 1.6   | 35.7  | 1.1   | 36.2  | 1.8   | 40.4  | 1.9   | 39.4  | 2.2   | 34.8  | 1.4   | 34.1  | 1.7   |
| Pyrope  | 24.9  | 1.9   | 30.3  | 0.7   | 34.8  | 1     | 31.8  | 0.7   | 23.4  | 1.3   | 27.1  | 0.9   | 36.9  | 1.8   | 36    | 1.8   |
| Grossular                                       | 27.3  | 0.9   | 24    | 0.9   | 21.9  | 0.7   | 25.7  | 0.8   | 29.6  | 1.4   | 28.3  | 1.7   | 21.2  | 1     | 23.2  | 1.1   |

| Run no.:                       | MS11  |      |       |      | MS24  |      |       |      | PEL1  |      |       |      |
|--------------------------------|-------|------|-------|------|-------|------|-------|------|-------|------|-------|------|
| P (GPa):                       | 3     |      |       |      | 3     |      |       |      | 3     |      |       |      |
| T (°C):                        | 900   |      |       |      | 950   |      |       |      | 900   |      |       |      |
| H <sub>2</sub> O (wt %):       | 8.1   |      |       |      | 7.3   |      |       |      | 8.5   |      |       |      |
| S (wt %):                      | 2     |      |       |      | 2     |      |       |      | 1     |      |       |      |
|                                | Core  |      | Rim   |      | Core  |      | Rim   |      | Core  |      | Rim   |      |
| Analyses:                      | 2     | SD   | 4     | SD   | 6     | SD   | 9     | SD   | 9     | SD   | 9     | SD   |
| <i>wt % oxide</i>              |       |      |       |      |       |      |       |      |       |      |       |      |
| SiO <sub>2</sub>               | 38.55 | 0.01 | 38.5  | 0.58 | 38.24 | 0.76 | 38.09 | 0.59 | 38.08 | 1.02 | 39.25 | 0.36 |
| TiO <sub>2</sub>               | 1.38  | 0.32 | 1.39  | 0.66 | 1.8   | 0.15 | 1.21  | 0.08 | 0.88  | 0.21 | 0.61  | 0.1  |
| Al <sub>2</sub> O <sub>3</sub> | 20.88 | 0.6  | 21.04 | 0.36 | 18.98 | 0.96 | 19.97 | 0.34 | 23.07 | 1.32 | 21.89 | 0.26 |
| FeO                            | 20.72 | 0.19 | 20.16 | 0.86 | 18.75 | 0.78 | 19.3  | 0.51 | 23.49 | 1.3  | 23.2  | 0.83 |

(continued)



Table 3: Continued

| Run no.:  | MS11  |       |       |       | MS24  |       |       |       | PEL1  |       |       |       |
|---|-------|-------|-------|-------|-------|-------|-------|-------|-------|-------|-------|-------|
| <i>P</i> (GPa):                                 | 3     |       |       |       | 3     |       |       |       | 3     |       |       |       |
| <i>T</i> (°C):                                  | 900   |       |       |       | 950   |       |       |       | 900   |       |       |       |
| H <sub>2</sub> O (wt %):                        | 8.1   |       |       |       | 7.3   |       |       |       | 8.5   |       |       |       |
| S (wt %):                                       | 2     |       |       |       | 2     |       |       |       | 1     |       |       |       |
|   | Core  |       | Rim   |       | Core  |       | Rim   |       | Core  |       | Rim   |       |
| Analyses:                                       | 2     | SD    | 4     | SD    | 6     | SD    | 9     | SD    | 9     | SD    | 9     | SD    |
| MnO   | 0.7   | 0.05  | 0.65  | 0.08  | 0.7   | 0.18  | 0.57  | 0.1   | 0.5   | 0.06  | 0.41  | 0.2   |
| MgO   | 8.92  | 0.03  | 8.99  | 0.16  | 10.54 | 0.14  | 10.39 | 0.23  | 12.63 | 1.36  | 13.63 | 0.56  |
| CaO   | 7.63  | 0.53  | 8.24  | 0.74  | 8.53  | 0.83  | 8.17  | 0.35  | 0.39  | 0.04  | 0.44  | 0.05  |
| Na <sub>2</sub> O                               | 0.13  | 0.09  | 0.09  | 0.05  | 0.16  | 0.1   | 0.09  | 0.05  | 0.02  | 0.02  | 0.03  | 0.02  |
| Total   | 98.9  | 0.55  | 99.07 | 0.69  | 97.72 | 0.52  | 97.8  | 0.93  | 99.07 | 0.6   | 99.48 | 0.69  |
| <i>Structural formula (based on 12 oxygens)</i> |       |       |       |       |       |       |       |       |       |       |       |       |
| Si  | 2.973 | 0.005 | 2.961 | 0.032 | 2.979 | 0.062 | 2.963 | 0.029 | 2.899 | 0.059 | 2.968 | 0.016 |
| Ti  | 0.08  | 0.019 | 0.08  | 0.038 | 0.105 | 0.009 | 0.071 | 0.005 | 0.051 | 0.013 | 0.034 | 0.005 |
| Al <sub>tot</sub>                               | 1.898 | 0.057 | 1.907 | 0.023 | 1.743 | 0.084 | 1.831 | 0.024 | 2.07  | 0.122 | 1.951 | 0.015 |
| Fe <sub>tot</sub>                               | 1.336 | 0.01  | 1.297 | 0.063 | 1.222 | 0.049 | 1.255 | 0.036 | 1.497 | 0.097 | 1.468 | 0.058 |
| Mn  | 0.046 | 0.003 | 0.042 | 0.005 | 0.046 | 0.012 | 0.038 | 0.006 | 0.032 | 0.004 | 0.026 | 0.013 |
| Mg  | 1.025 | 0.005 | 1.031 | 0.016 | 1.225 | 0.013 | 1.205 | 0.028 | 1.433 | 0.142 | 1.536 | 0.054 |
| Ca  | 0.63  | 0.043 | 0.679 | 0.058 | 0.712 | 0.071 | 0.681 | 0.027 | 0.032 | 0.003 | 0.036 | 0.004 |
| Na  | 0.019 | 0.014 | 0.014 | 0.007 | 0.024 | 0.015 | 0.014 | 0.008 | 0.004 | 0.004 | 0.005 | 0.003 |
| Total   | 8.008 |       | 8.012 |       | 8.055 |       | 8.057 |       | 8.017 |       | 8.024 |       |
| Mg#   | 0.43  | 0     | 0.44  | 0.01  | 0.5   | 0.01  | 0.49  | 0.01  | 0.49  | 0.04  | 0.51  | 0.02  |
| Spessartine                                     | 1.5   | 0.1   | 1.4   | 0.2   | 1.4   | 0.4   | 1.2   | 0.2   | 1.1   | 0.1   | 0.9   | 0.4   |
| Almandine                                       | 42.8  | 2.1   | 40.9  | 1.5   | 31.8  | 2.4   | 33.9  | 1.3   | 49.1  | 4.6   | 45.7  | 1.7   |
| Pyrope  | 33.8  | 0.7   | 33.8  | 0.5   | 38.2  | 0.5   | 37.9  | 1     | 47.8  | 3.8   | 50.1  | 1.8   |
| Grossular                                       | 20.7  | 1.1   | 22.3  | 2     | 22.2  | 2.1   | 21.4  | 0.8   | 1.1   | 0.1   | 1.2   | 0.1   |

The ‘analyses’ row refers to the number of analyses used to calculate the average. SD, standard deviation. Mg# = Mg/(Mg + Fe).

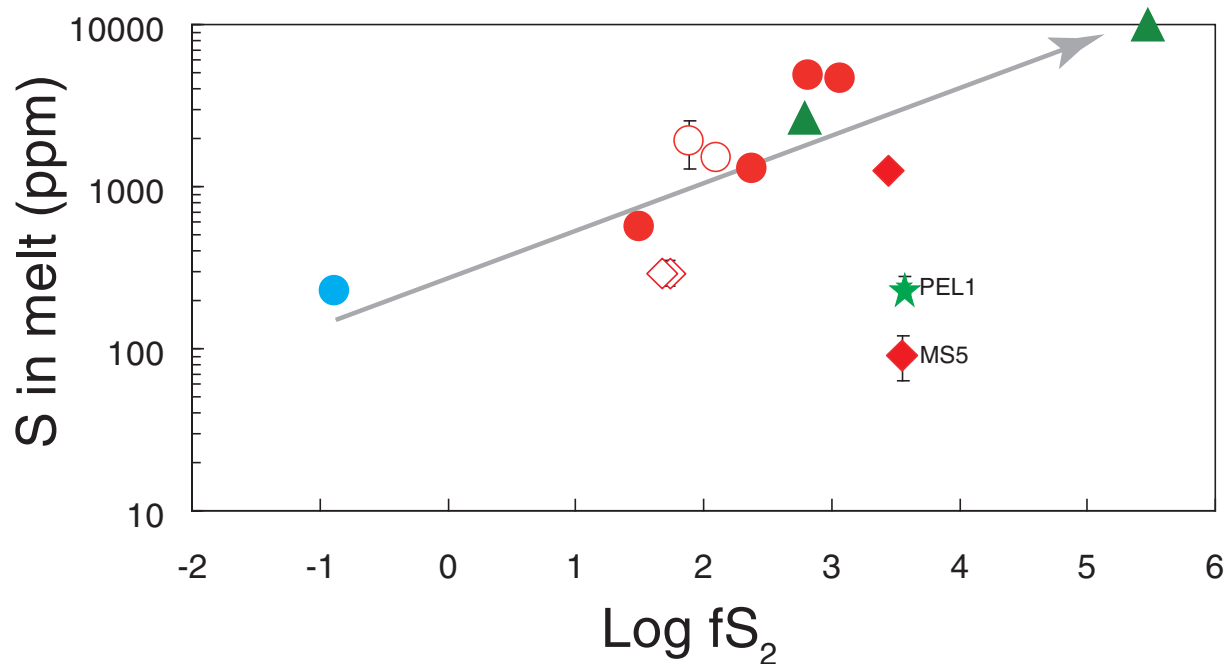
(Table 3). Hydrous silicate glass (quenched liquid) is present in all experimental charges, displaying a clean texture. Glass occurs evenly throughout charges, although some local concentrations are apparent near the tip of the capsule. Small, micron-sized, vesicles occur in some quenched glasses, in particular those from crystal-rich basalt charges (Fig. 3b and c). We interpret these as resulting from fluid exsolution upon quench. In pelite-derived charges, however, quench glasses are free of any, even submicroscopic, bubbles (Fig. 3d), supporting the idea that our run products have, in general, been cooled at a rate fast enough to avoid profuse quench effects (Hermann & Spandler, 2008). In particular, we did not find textures similar to those described by Klimm *et al.* (2008), where run products showed a strongly vesicular, glassy matrix, interpreted as arising from unmixing upon quenching of a supercritical fluid or melt. In accord with Schmidt *et al.* (2004), Hermann *et al.* (2006) and Hermann & Spandler (2008), we conclude that the pelite experiments are all undersaturated

in water at the conditions investigated and are therefore fully quenchable to a glass.

### Basaltic system

In the basaltic system at 2 GPa, phases identified in addition to glass are amphibole, pyroxene, Fe–Ti oxides, anhydrite and sulphide (Table 2). Amphibole is stable at all investigated temperatures (800–950°C). In contrast, clinopyroxene is present only at 950°C, whereas it is stable at 900°C in sulphur-free basaltic systems at equivalent conditions (Prouteau *et al.*, 2001). At 3 GPa, the mineral assemblage is dominated by garnet and clinopyroxene associated with rutile, Fe–Ti oxides, anhydrite and sulphide. In addition, apatite, epidote and coesite are present in the low-temperature runs and orthopyroxene is stable at 950°C. Amphibole is stable at 700 and 800°C in the 2 wt % S experiments.

Phase proportions were determined for the 3 GPa and 900°C charges, using average phase compositions and



- | MOR basalt                                 | Pelitic oceanic sediment |
|--|--------------------------|
| ◇ 1 wt% S, 2 GPa                           | ★ 1 wt% S, 3 GPa         |
| ◆ 1 wt% S, 3 GPa                           | ▲ 4 wt% S, 3 GPa         |
| ○ 2 wt% S, 2 GPa                           |                          |
| ● 2 wt% S, 3 GPa                           |                          |
| ● 2 wt% S, 3 GPa,<br>(reducing conditions) |                          |

**Fig. 2.** Co-variation between  $\log fS_2$  and the sulphur content of the glasses of the experimental charges. The  $fS_2$  values are calculated following the methods of Bockrath *et al.* (2004) and Liu *et al.* (2007).

least-squares regressions. Under these conditions, an increase in the sulphur content in the system leads to an increase in glass abundance and a decrease in clinopyroxene abundance (Fig. 4).

#### *Pelitic system*

In the pelitic system, major silicate phases include aluminium silicate, garnet or orthopyroxene, and rutile and sulphide as ubiquitous minor phases. Phlogopite and coesite are present at 800°C, but absent at 900°C. The lack of anhydrite is interpreted to result from the CaO-poor character of the pelite. No phengite was detected.

## PHASE COMPOSITIONS

### Garnet

In the basaltic system, all runs performed at 3 GPa contained abundant euhedral poikilitic garnet (50–500  $\mu\text{m}$ ),

with abundant inclusions of clinopyroxene, sulphide, rutile, and anhydrite (Fig. 3). Garnets are often enriched in Ti in their cores, whereas Mg (or Ca) is enriched in the rims (Table 3). These cores are interpreted to represent garnet growth before complete equilibrium was reached. Our interpretation is based on garnet rim compositions, as they are likely to be close to equilibrium with the matrix. All garnets contain significant amounts of  $\text{TiO}_2$  (>1 wt %) and  $\text{Na}_2\text{O}$  ranges from 0.08 to 0.12 wt %.

The calculation of structural formulae reveals that garnets display essentially almandine–pyrope compositions (67–75%) with significant (>20%) grossular, whereas spessartine remains low, <2%. The most significant feature is an increase of pyrope content and Mg-number [ $\text{Mg}/(\text{Fe}_{\text{tot}} + \text{Mg})$  in moles, hereafter referred to as Mg#], and a decrease in grossular content with increasing temperature, for given total sulphur content in the system (Fig. 5a). At fixed  $T$ , the Mg# increases significantly with

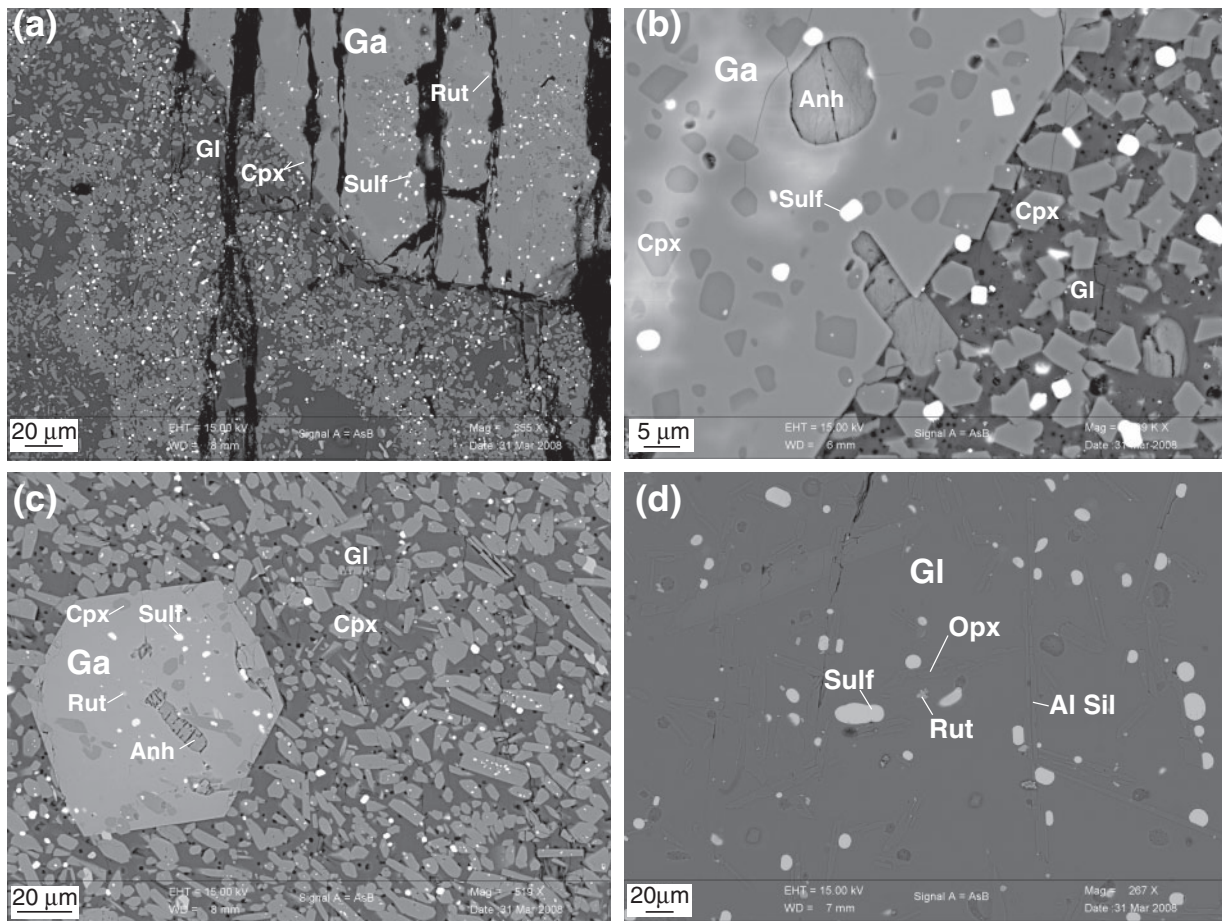


**Fig. 3.** Back-scattered electron images of basaltic charges: (a) MS11, 900°C and 3 GPa, reducing conditions; (b) MS9, 900°C and 3 GPa, oxidizing conditions; (c) MS10, 800°C and 3 GPa, oxidizing conditions. (d) Pelitic charge, PEL2, 900°C and 3 GPa, oxidizing conditions. A micrometre scale bar is shown in the lower left corner of each image. The clean aspect of the glass in the pelite charge should be noted, whereas the basaltic ones display sub-micron-sized bubbles of inferred quench origin. Gl, glass; Ga, garnet; Cpx, clinopyroxene; Opx, orthopyroxene; Al sil, aluminium silicate; Rut, rutile; Anh, anhydrite; Sulf, sulphide.

the total sulphur content (Fig. 5a): from 0.36 in a sulphur-free system at 900°C (Prouteau *et al.*, 2001) to 0.48 with 2 wt % S added (Fig. 5a). At 800°C, this effect is, however, less clear. For a given temperature and total sulphur content, decreasing  $fO_2$  decreases pyrope and increases almandine contents (compare MS9 and MS11, Table 3).

Titanium concentrations are lower than in sulphur-free experiments (Fig. 5b). In the pelitic composition, garnet is present only in the charge loaded with 1 wt % sulphur at 900°C, displaying a pyrope–almandine composition, with Mg-number  $\sim 0.5$  and spessartine  $\sim 1\%$ . Compared with garnets synthesized at 2.5–3.5 GPa in a sulphur-free pelite (Hermann & Spandler, 2008), the garnet in run PEL1 has a significantly higher Mg# (Fig. 5a). Titanium concentration is low (0.61%) and falls in the range observed in sulphur-free experiments (Hermann & Spandler, 2008) (Fig. 5b).

### Amphibole

Amphibole is stable at all investigated conditions at 2 GPa in the basaltic system. It is not found at 3 GPa with 1.1 wt % S, and is not stable over 800°C in the most sulphur-rich charges at 3 GPa. Amphibole forms subhedral to euhedral grains ranging from a few microns up to 200  $\mu\text{m}$  for the higher temperature runs.

The amphibole composition appears to be homogeneous on the basis of several grains in each charge and an average amphibole composition is reported in Table 4. It is a calcic and aluminous amphibole, classified as magnesiohornblende or tschermakitic hornblende (Leake *et al.*, 1997). Structural formulae are calculated on the basis of 23 oxygens. The Mg# ranges between 0.57 and 0.72, being insensitive to temperature at fixed pressure and total sulphur content. The effect of bulk sulphur content on Mg# is difficult to assess. However, at 2 GPa and 900°C, the Mg# increases from 0.64 in a sulphur-free

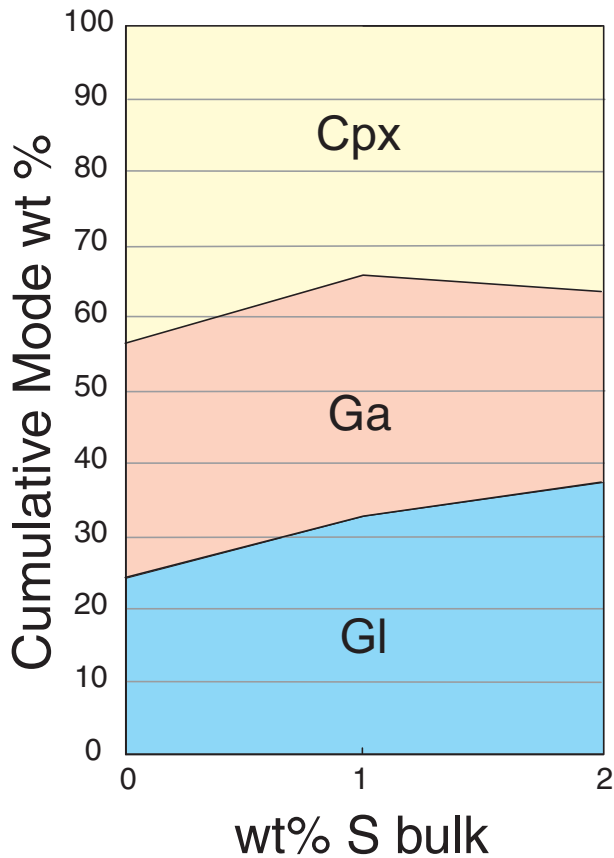


**Fig. 4.** Cumulative modes (calculated from mass balance on the major oxides) for 3 GPa and 900°C experimental charges plotted against total sulphur content in the system. Data from this study and Prouteau *et al.* (2001).

system (Prouteau *et al.* 2001) to 0.72 with 2 wt % sulphur added (Fig. 6a). This suggests a positive correlation of amphibole Mg# with total sulphur content.

The Ti content varies from 0.12 to 0.28 p.f.u. (per formula unit). Titanium concentrations show no clear correlation with sulphur content (Fig. 6b). At a fixed pressure and bulk sulphur content, increasing temperature results in an increase in Ti content (Fig. 6b). The partition coefficient (in wt %) varies between 2.2 and 6.2 (Table 4) and shows a strong negative correlation with temperature (Fig. 6c), being relatively insensitive to the presence or absence of sulphur.

### Clinopyroxene

Clinopyroxene, identified only in the basaltic composition, generally forms small grains (micron-sized to  $\sim 10 \mu\text{m}$ ) that are sometimes difficult to analyse (Table 5). Clinopyroxene is present only at 950°C at 2 GPa and at temperatures  $\geq 800^\circ\text{C}$  at 3 GPa. Clinopyroxene produced in oxidizing conditions at 3 GPa has a 18–20 wt % CaO,

1–2 wt %  $\text{Na}_2\text{O}$ , and 6.4–7.6 wt %  $\text{Al}_2\text{O}_3$ . Clinopyroxene in the 2 GPa experiment lacking garnet contains more  $\text{TiO}_2$  (1.6 wt %) and less  $\text{Na}_2\text{O}$  (0.6 wt %). Clinopyroxene produced at 3 GPa in reducing conditions (MSII) is characterized by significantly higher  $\text{Al}_2\text{O}_3$  (11 wt %) and lower CaO (15 wt %) contents. Its Mg# ranges between 0.62 and 0.75. At 3 GPa and 2 wt % bulk S, a rise in temperature produces a significant increase in Mg# (Fig. 7a). The experimental results also suggest that adding sulphur increases the clinopyroxene Mg#, as already noticed for both garnet and, to a lesser extent, amphibole. For example, clinopyroxene produced at 3 GPa and 900°C in the sulphur-free experiments of Prouteau *et al.* (2001) has a lower Mg# (0.58) than those synthesized in the 2 wt % sulphur-added experiments (Mg# = 0.70), all other parameters being similar (Table 5, Fig. 7a). In contrast, Na, Ca, Ti and Al contents show no systematic variations with varying temperature or bulk S content within analytical error (Table 5 and Fig. 7b and c).

### Orthopyroxene

Orthopyroxene was identified at 950°C in the basaltic system with 2 wt % total sulphur content. Large grains ( $>50 \mu\text{m}$ ) of orthopyroxene are distributed heterogeneously in these experimental charges. Orthopyroxene produced at 3 GPa is more aluminous ( $\text{Al}_2\text{O}_3 = 5.7 \text{ wt } \%$ ) at 3 GPa than at 2 GPa ( $\text{Al}_2\text{O}_3 = 3.1 \text{ wt } \%$ ). Its Mg# is 0.80 at 2 GPa, slightly decreasing to 0.77 at 3 GPa (Table 6). Orthopyroxene occurs also in the pelitic charges with 4 wt % sulphur added (garnet is absent in these charges). Orthopyroxene is aluminous ( $\text{Al}_2\text{O}_3 = 8.3\text{--}9.1 \text{ wt } \%$ ). Its Mg# is high and increases slightly with temperature (0.92 at 800°C, 0.96 at 900°C).

### Biotite

Biotite is present in only one 800°C charge in the pelitic system (PEL3, Table 7). It contains 1.9 wt %  $\text{TiO}_2$  and 0.2 wt %  $\text{Na}_2\text{O}$  and has a high Mg# (0.91, Table 7). For comparison, the Mg# range of biotite produced in the sulphur-free experiments of Hermann & Spandler (2008) ranges between 0.71 and 0.78 (2.5 GPa, 750–900°C).

### Melt

Table 8 presents glass compositions from the experiments normalized to 100 wt % on an anhydrous basis. The water contents of the quenched glasses estimated by the by-difference approach (see Analytical techniques) fall in the range 7–14 wt % (Table 8). The occasional presence of submicron-size bubbles in the basalt charges suggests, however, that such estimates are minima. Estimation based on mass-balance calculations using  $\text{K}_2\text{O}$  is possible in charges whose phase assemblages lack  $\text{K}_2\text{O}$ -rich and/or hydrous minerals (amphibole, biotite). In this case,  $\text{K}_2\text{O}$  behaviour is largely incompatible during melting, and its concentration in the matrix glass can be used to calculate the

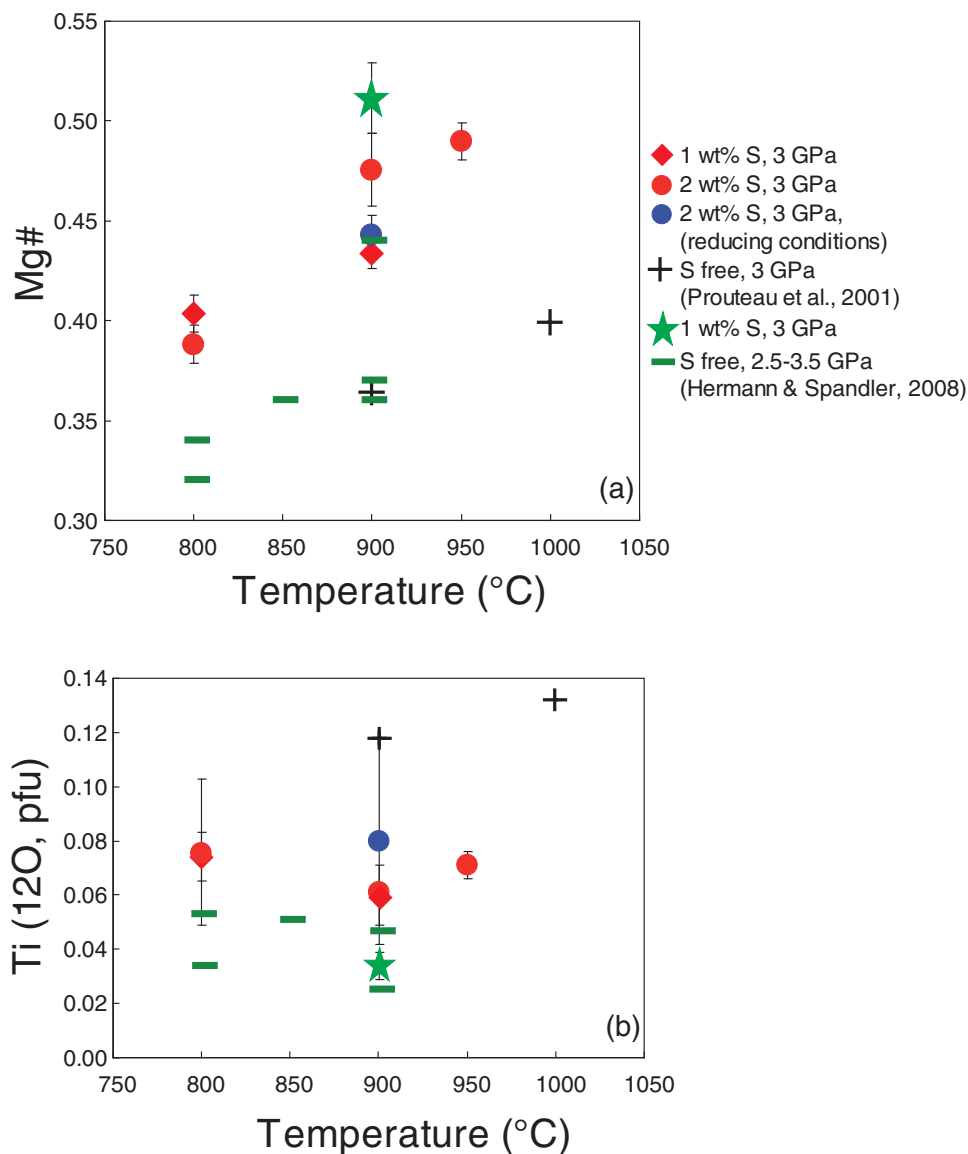


**Fig. 5.** Variation of experimental garnet compositions with temperature: (a) Mg#; (b) Ti. Errors bars represent 1 standard deviation of multiple mineral analyses.

minimum amount of residual glass, which in turn allows us to retrieve the maximum amount of dissolved water (again assuming incompatible behaviour for H<sub>2</sub>O). The full range of restored dissolved H<sub>2</sub>O is 11–31 wt % (Table 8), the highest value being close to the H<sub>2</sub>O solubility determined at 4 GPa (Kessel *et al.*, 2005b). However, most charges have dissolved water contents of 11–20 wt %, in some cases being considerably higher than that given by-difference, corroborating the fact that some water may have been exsolved during quench. It should be noted that the presence of CO<sub>2</sub> may also have promoted the formation of a fluid phase in the pelite experiments, which could have scavenged some of the water, and other

elements, particularly Na. Regardless, we stress that this range of H<sub>2</sub>O contents is at least twice the solubility of H<sub>2</sub>O in silicate melts at 0.2 GPa; that is, much higher than in low-pressure experimental studies of sulphur solubility in silicic melts (Carroll & Rutherford, 1988; Luhr, 1990; Carroll & Webster, 1994; Scaillet & Evans, 1999; Clemente *et al.*, 2004; Costa *et al.*, 2004; Parat *et al.*, 2008).

#### Major element characteristics

Glasses produced in basaltic charges are metaluminous to slightly peraluminous ( $0.87 < ASI < 1.27$ ) with SiO<sub>2</sub> contents between 60 and 73 wt %. At a fixed pressure and bulk sulphur content, the glasses show decreasing SiO<sub>2</sub>

Table 4: Experimental amphibole compositions

| Run no.:  | MS7    |       | MS6    |       | MS26   |       | MS29   |       | MS22   |       | MS10   |       |
|---|--------|-------|--------|-------|--------|-------|--------|-------|--------|-------|--------|-------|
| <i>P</i> (GPa):                                 | 2      |       | 2      |       | 2      |       | 2      |       | 3      |       | 3      |       |
| <i>T</i> (°C):                                  | 800    |       | 900    |       | 900    |       | 950    |       | 700    |       | 800    |       |
| H <sub>2</sub> O (wt %):                        | 6.7    |       | 6.6    |       | 6      |       | 6.5    |       | 6.8    |       | 6.6    |       |
| S (wt %):                                       | 1.1    |       | 1.1    |       | 2      |       | 2      |       | 2      |       | 2      |       |
| Analyses:                                       | 6      | SD    | 11     | SD    | 6      | SD    | 4      | SD    | 9      | SD    | 13     | SD    |
| <i>wt % oxide</i>                               |        |       |        |       |        |       |        |       |        |       |        |       |
| SiO <sub>2</sub>                                | 43.92  | 1.28  | 40.31  | 0.58  | 43.38  | 0.80  | 42.53  | 0.34  | 45.66  | 1.51  | 42.83  | 0.77  |
| TiO <sub>2</sub>                                | 1.95   | 0.37  | 2.52   | 0.24  | 2.10   | 0.14  | 2.50   | 0.14  | 1.05   | 0.32  | 1.38   | 0.40  |
| Al <sub>2</sub> O <sub>3</sub>                  | 10.87  | 0.72  | 13.31  | 0.63  | 12.50  | 0.71  | 12.42  | 0.54  | 12.30  | 0.63  | 14.27  | 0.42  |
| FeO   | 12.41  | 0.78  | 14.90  | 0.71  | 9.73   | 0.45  | 9.77   | 0.44  | 12.49  | 0.74  | 14.33  | 0.80  |
| MnO   | 0.28   | 0.05  | 0.26   | 0.11  | 0.16   | 0.07  | 0.27   | 0.13  | 0.23   | 0.09  | 0.25   | 0.11  |
| MgO   | 11.79  | 0.81  | 11.39  | 0.46  | 14.14  | 0.51  | 14.22  | 0.66  | 10.30  | 0.79  | 10.84  | 0.33  |
| CaO   | 10.79  | 0.22  | 10.09  | 0.39  | 10.75  | 0.30  | 11.37  | 0.99  | 9.78   | 0.64  | 9.85   | 0.34  |
| Na <sub>2</sub> O                               | 1.82   | 0.12  | 2.53   | 0.13  | 2.51   | 0.18  | 2.38   | 0.20  | 2.74   | 0.66  | 2.34   | 0.11  |
| K <sub>2</sub> O                                | 0.15   | 0.03  | 0.16   | 0.05  | 0.21   | 0.05  | 0.15   | 0.03  | 0.26   | 0.07  | 0.23   | 0.05  |
| Total   | 93.99  | 0.52  | 95.48  | 0.91  | 95.47  | 0.76  | 95.62  | 0.75  | 94.80  | 1.36  | 96.32  | 0.85  |
| <i>Structural formula (based on 23 oxygens)</i> |        |       |        |       |        |       |        |       |        |       |        |       |
| Si  | 6.601  | 0.186 | 5.985  | 0.081 | 6.333  | 0.087 | 6.230  | 0.109 | 6.801  | 0.172 | 6.254  | 0.130 |
| Ti  | 0.220  | 0.042 | 0.282  | 0.027 | 0.231  | 0.016 | 0.276  | 0.020 | 0.118  | 0.036 | 0.151  | 0.043 |
| Al <sub>tot</sub>                               | 1.925  | 0.129 | 2.329  | 0.097 | 2.150  | 0.122 | 2.143  | 0.061 | 2.159  | 0.097 | 2.455  | 0.073 |
| Fe <sub>tot</sub>                               | 1.560  | 0.099 | 1.850  | 0.091 | 1.188  | 0.056 | 1.197  | 0.040 | 1.557  | 0.098 | 1.749  | 0.089 |
| Mn  | 0.036  | 0.007 | 0.033  | 0.014 | 0.020  | 0.009 | 0.033  | 0.016 | 0.029  | 0.012 | 0.031  | 0.014 |
| Mg  | 2.640  | 0.178 | 2.521  | 0.103 | 3.077  | 0.111 | 3.104  | 0.092 | 2.288  | 0.174 | 2.360  | 0.063 |
| Ca  | 1.738  | 0.041 | 1.606  | 0.067 | 1.681  | 0.045 | 1.787  | 0.186 | 1.561  | 0.108 | 1.541  | 0.057 |
| Na  | 0.531  | 0.036 | 0.729  | 0.036 | 0.710  | 0.051 | 0.677  | 0.052 | 0.791  | 0.195 | 0.662  | 0.035 |
| K   | 0.029  | 0.006 | 0.031  | 0.010 | 0.038  | 0.010 | 0.028  | 0.006 | 0.050  | 0.013 | 0.042  | 0.009 |
| Σcations  | 15.280 |       | 15.365 |       | 15.429 |       | 15.475 |       | 15.354 |       | 15.245 |       |
| Mg#   | 0.63   | 0.01  | 0.58   | 0.02  | 0.72   | 0.01  | 0.72   | 0.01  | 0.60   | 0.01  | 0.57   | 0.01  |
| <i>DTiO</i> <sub>2</sub> (wt %)                 | 4.1    |       | 3.5    |       | 2.5    |       | 2.2    |       | 6.2    |       | 4.2    |       |
| <i>DK</i> <sub>2</sub> O (wt %)                 | 0.17   |       | 0.28   |       | 0.35   |       | 0.34   |       | 0.31   |       | 0.38   |       |

The ‘analyses’ row refers to the number of analyses used to calculate the average. SD, standard deviation. Mg# = Mg/(Mg + Fe<sub>tot</sub>); *DK*<sub>2</sub>O = K<sub>2</sub>O (wt %) amphibole/K<sub>2</sub>O (wt %) melt; *DTiO*<sub>2</sub> = TiO<sub>2</sub> (wt %) amphibole/TiO<sub>2</sub> (wt %) melt.

and increasing FeO, MgO and TiO<sub>2</sub> with increasing temperature (Table 8, Fig. 8). The melts have low TiO<sub>2</sub> contents, generally below 1 wt %, and  $X_{Mg}$  [Mg/(Mg + Fe)] ranging from 0.21 to 0.46, in general in the range 0.30–0.40.

The CIPW (wt %) normative components of the glasses produced at 2 and 3 GPa have been projected into an Ab–An–Or triangular diagram in Fig. 9. For comparison, the compositions of melts produced from partial melting of hydrous basalt (Prouteau *et al.*, 2001) without sulphur are also shown. Melt compositions from S-bearing basaltic charges have low orthoclase components, a reflection of their low K contents, and trend away from the

trondhjemite field towards the tonalite field in this projection (Fig. 9). Increasing temperature and/or increasing total sulphur content in the system increases the An contents of the partial melts.

In pelitic charges, all glasses have silicic compositions, being strongly peraluminous with a very low FeO\*/MgO, and MgO contents up *c.* 2 wt %. The elevated MgO content is a remarkable feature of the experimental melts, with the Mg# ranging from 0.66 to 0.97. Pelite-derived melts with sulphur fall in the granitic field of the Ab–An–Or diagram, contrasting with the trondhjemitic compositions obtained in similar low-temperature (800°C), but S-free, experiments (Fig. 9). It should be noted

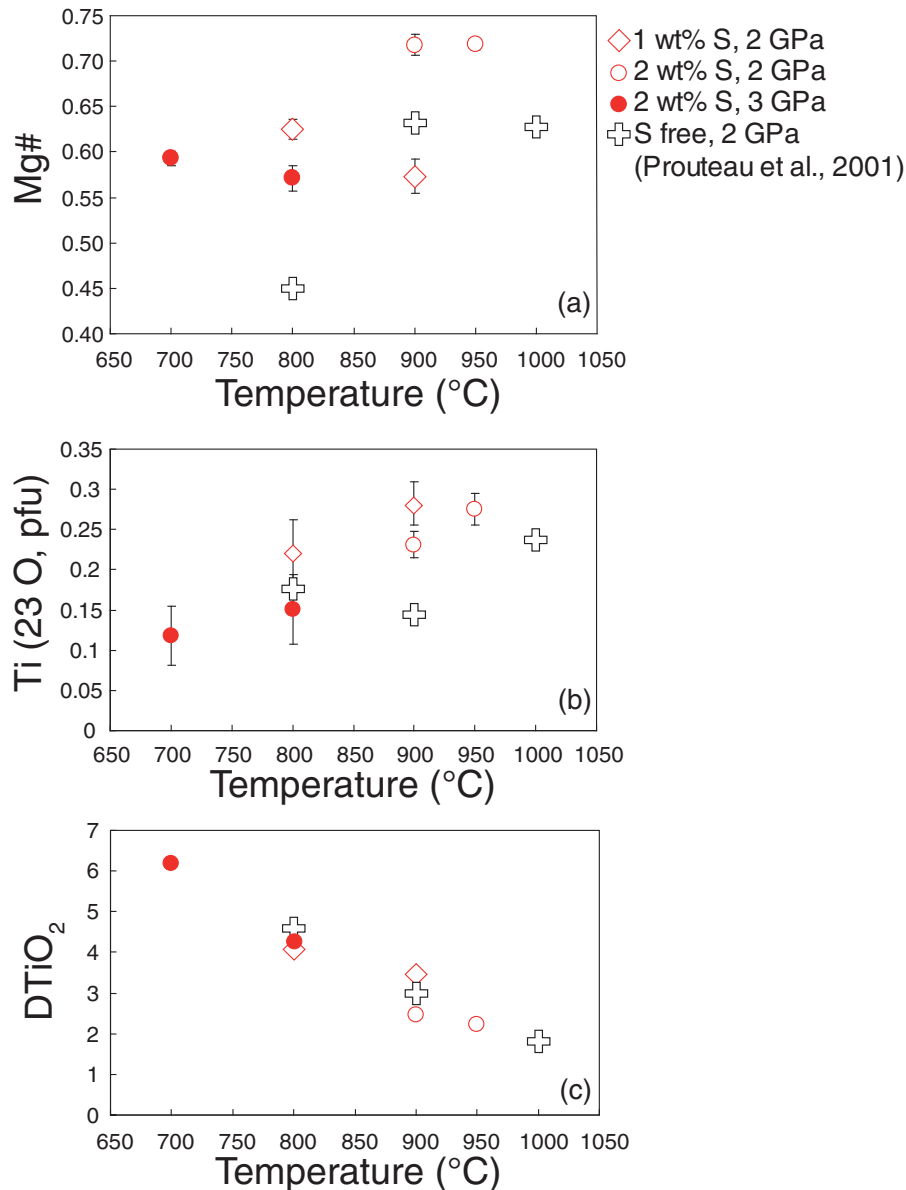


**Fig. 6.** Variation of experimental amphibole composition with temperature: (a) Mg#; (b) Ti; (c) DTiO<sub>2</sub>. Errors bars (a, b) represent 1 standard deviation of multiple mineral analyses.

that the composition of Hermann & Spandler (2008) has slightly less H<sub>2</sub>O: 6.8 wt % instead of 8.5 wt % H<sub>2</sub>O in our pelite, which could affect the phase relationships (see discussion below). The potassium-rich character reflects the lack of phengite in our charges, and perhaps Na<sub>2</sub>O scavenging towards the fluid, if any.

#### Melt sulphur contents

Figure 10 shows the analysed sulphur contents of our quenched glasses, compared with those of silicic melts (SiO<sub>2</sub> >60 wt %) also saturated in sulphide and/or sulphate phases but synthesized at pressures <0.4 GPa (Luhr,

1990; Carroll & Webster, 1994; Scaillet *et al.*, 2003; Wallace, 2005). For the latter, all experimental data indicate that at around 700°C, the sulphur content of silicic melts is at or below 50 ppm, and hardly exceeds 150 ppm at 800°C (Fig. 10).

The glasses obtained at 2 and 3 GPa, 800°C and NNO +1 with 1 wt % added sulphur have sulphur contents higher by a factor of two relative to those at lower pressures (Fig. 10). Increasing temperature to 900°C has no detectable effect at 2 GPa, whereas at 3 GPa it raises the melt S content to over 1000 ppm. At both 2 and 3 GPa, increasing the bulk S content to 2 wt % increases the amount of

Table 5: Experimental clinopyroxene compositions

| Run no.:                                       | MS29  |       | MS5   |       | MS1   |       | MS10  |       | MS9   |       | MS11  |       | MS24  |  |
|--|-------|-------|-------|-------|-------|-------|-------|-------|-------|-------|-------|-------|-------|--|
| $P$ (GPa):                                     | 2     |       | 3     |       | 3     |       | 3     |       | 3     |       | 3     |       | 3     |  |
| $T$ ( $^{\circ}\text{C}$ ):                    | 950   |       | 800   |       | 900   |       | 800   |       | 900   |       | 900   |       | 950   |  |
| $\text{H}_2\text{O}$ (wt %):                   | 6.5   |       | 6.2   |       | 5.4   |       | 6.6   |       | 5.4   |       | 8.1   |       | 7.3   |  |
| $\text{S}$ (wt %):                             | 2     |       | 1.1   |       | 1.1   |       | 2     |       | 2     |       | 2     |       | 2     |  |
| Analyses:                                      | 2     | SD    | 8     | SD    | 9     | SD    | 1     | 6     | SD    | 10    | SD    | 5     | SD    |  |
| <i>wt % oxide</i>                              |       |       |       |       |       |       |       |       |       |       |       |       |       |  |
| $\text{SiO}_2$                                 | 48.55 | 0.59  | 49.28 | 1.45  | 49.87 | 1.12  | 47.61 | 49.59 | 0.56  | 49.45 | 1.33  | 49.34 | 0.43  |  |
| $\text{TiO}_2$                                 | 1.64  | 0.13  | 0.63  | 0.28  | 0.75  | 0.18  | 0.91  | 0.77  | 0.05  | 0.91  | 0.27  | 0.89  | 0.13  |  |
| $\text{Al}_2\text{O}_3$                        | 5.97  | 0.63  | 6.41  | 1.61  | 7.34  | 1.20  | 7.88  | 7.62  | 0.46  | 11.05 | 1.61  | 7.27  | 0.60  |  |
| $\text{FeO}$                                   | 8.79  | 0.08  | 8.49  | 1.48  | 9.44  | 0.76  | 10.54 | 8.94  | 0.69  | 9.36  | 1.18  | 7.71  | 0.48  |  |
| $\text{MnO}$                                   | 0.16  | 0.15  | 0.18  | 0.09  | 0.16  | 0.09  | 0.24  | 0.24  | 0.09  | 0.23  | 0.11  | 0.15  | 0.08  |  |
| $\text{MgO}$                                   | 13.83 | 0.80  | 11.40 | 1.10  | 10.93 | 0.54  | 9.79  | 11.78 | 0.40  | 10.47 | 0.72  | 12.97 | 0.74  |  |
| $\text{CaO}$                                   | 18.48 | 0.25  | 18.26 | 0.85  | 18.98 | 1.05  | 20.15 | 18.70 | 0.49  | 14.88 | 1.51  | 18.25 | 0.44  |  |
| $\text{Na}_2\text{O}$                          | 0.62  | 0.03  | 1.92  | 0.63  | 2.22  | 0.61  | 1.30  | 1.88  | 0.72  | 2.08  | 0.09  | 1.09  | 0.15  |  |
| Total  | 98.04 | 0.61  | 96.58 | 0.86  | 99.69 | 0.96  | 98.45 | 99.51 | 0.77  | 98.42 | 0.92  | 97.67 | 0.64  |  |
| <i>Structural formula (based on 6 oxygens)</i> |       |       |       |       |       |       |       |       |       |       |       |       |       |  |
| Si   | 1.836 | 0.010 | 1.889 | 0.045 | 1.862 | 0.031 | 1.819 | 1.849 | 0.016 | 1.838 | 0.033 | 1.857 | 0.007 |  |
| Ti   | 0.047 | 0.004 | 0.018 | 0.008 | 0.021 | 0.005 | 0.026 | 0.022 | 0.001 | 0.026 | 0.008 | 0.025 | 0.004 |  |
| Al   | 0.266 | 0.030 | 0.290 | 0.074 | 0.323 | 0.054 | 0.355 | 0.335 | 0.019 | 0.485 | 0.073 | 0.323 | 0.028 |  |
| Fe   | 0.278 | 0.005 | 0.273 | 0.049 | 0.295 | 0.024 | 0.337 | 0.279 | 0.020 | 0.291 | 0.038 | 0.243 | 0.015 |  |
| Mn   | 0.005 | 0.005 | 0.006 | 0.003 | 0.005 | 0.003 | 0.008 | 0.008 | 0.003 | 0.007 | 0.003 | 0.005 | 0.003 |  |
| Mg   | 0.780 | 0.040 | 0.651 | 0.060 | 0.608 | 0.027 | 0.558 | 0.655 | 0.025 | 0.580 | 0.037 | 0.728 | 0.038 |  |
| Ca   | 0.749 | 0.005 | 0.750 | 0.032 | 0.759 | 0.037 | 0.825 | 0.747 | 0.018 | 0.592 | 0.057 | 0.736 | 0.018 |  |
| Na   | 0.046 | 0.002 | 0.143 | 0.047 | 0.161 | 0.045 | 0.096 | 0.136 | 0.052 | 0.150 | 0.006 | 0.080 | 0.012 |  |
| Mg#  | 0.74  | 0.01  | 0.71  | 0.05  | 0.67  | 0.02  | 0.62  | 0.70  | 0.02  | 0.67  | 0.04  | 0.75  | 0.02  |  |

The ‘analyses’ row refers to the number of analyses used to calculate the average. SD, standard deviation. Mg# = Mg/(Mg + Fe).

dissolved sulphur by a factor of 10 relative to experimental solubilities determined at 0.2 GPa at equivalent temperatures. For instance, at 3 GPa, the melt in basaltic charges dissolves nearly 600 ppm sulphur at 700 $^{\circ}\text{C}$ , and over 1000 ppm at 800 $^{\circ}\text{C}$ . The most extreme sulphur content obtained in our study was achieved with the pelite loaded with 4 wt % sulphur at 3 GPa, conditions under which the silicate melt (with 75 wt %  $\text{SiO}_2$ ) dissolved nearly 1 wt % sulphur at 900 $^{\circ}\text{C}$  (Fig. 10), which is nearly two orders of magnitude more than at 0.2 GPa, under similar  $f\text{O}_2$  conditions. The critical role of  $f\text{O}_2$  in sulphur solubility is illustrated by the charge synthesized at 3 GPa, 2 wt % S bulk, 900 $^{\circ}\text{C}$  and NNO–2. In this charge, the silicate melt has a sulphur content of *c.* 200 ppm (Fig. 10), whereas that annealed at NNO + 1 resulted in *c.* 4600 ppm dissolved sulphur (i.e. 20 times more).

Melt sulphur contents are not correlated with melt FeO contents, as shown in Fig. 11. The lack of clear FeO control on S solubility in hydrous silicic melts has been already

pointed out by Clemente *et al.* (2004), and indicates that an elevated iron content is not crucial to achieve high dissolved sulphur (see below).

## DISCUSSION

### Effect of sulphur on phase relations and compositions

The addition of elemental sulphur to the experimental charges in relatively large amounts generally results in precipitation of sulphides (as long as  $f\text{O}_2$  is not too oxidizing); as a result, a significant part of the iron is ‘locked’ into sulphide, thereby decreasing the Fe/Mg of the rest of the system (liquid and Fe–Mg silicates). This has an impact on both phase compositions and stabilities. In particular, experimental ferromagnesian phases have systematically higher Mg#, compared with sulphur-free experiments, an observation previously made for lower pressure experiments (e.g. Scaillet & Evans, 1999; Costa *et al.*, 2004). It is



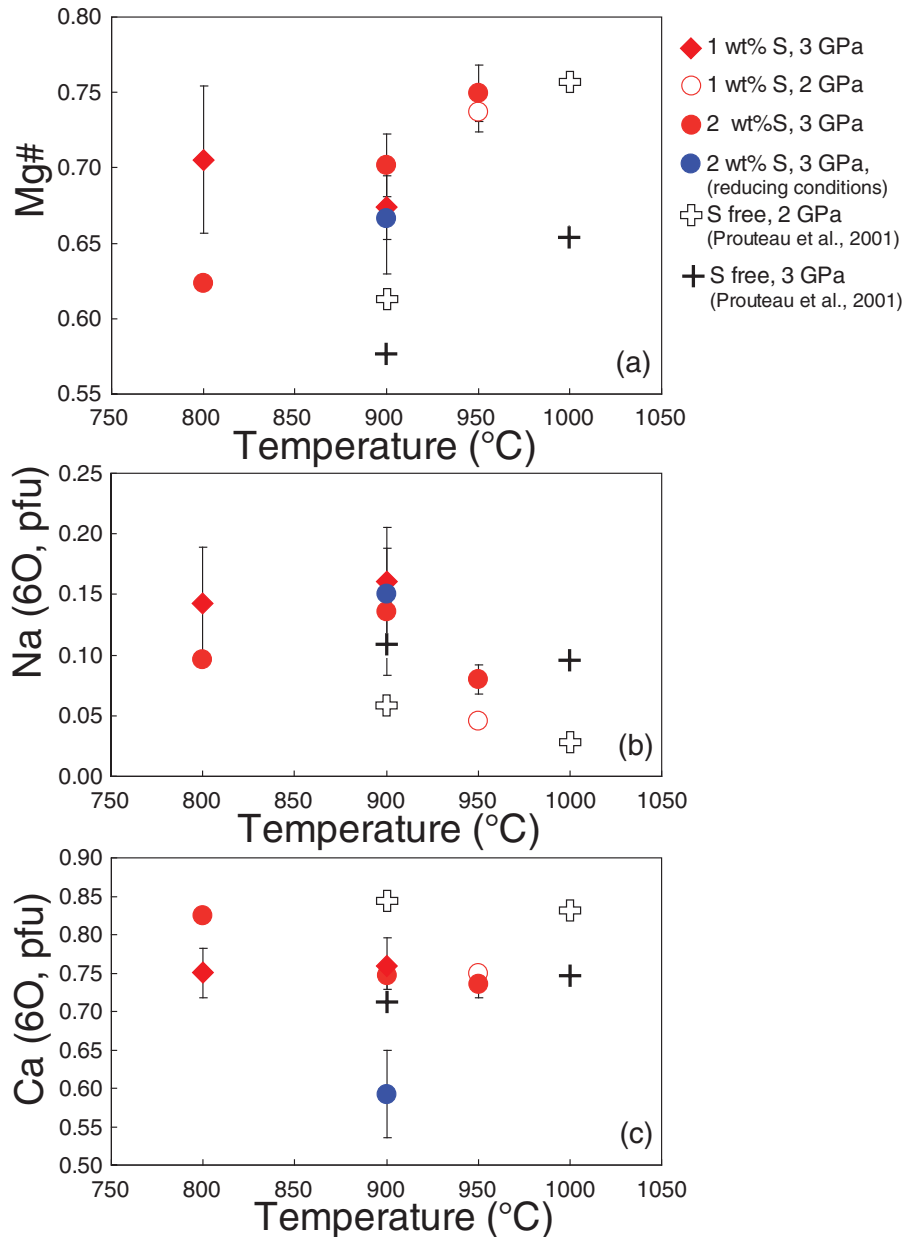


**Fig. 7.** Variation of experimental clinopyroxene compositions with temperature: (a) Mg#; (b) Na; (c) Ca. Errors bars represent 1 standard deviation of multiple mineral analyses.

important to note that the term sulphide is used here for either a solid or a liquid phase, whose composition is not necessarily stoichiometric FeS. It has long been known that pyrrhotite adjusts its composition to the prevailing  $f_{S_2}$  and most natural pyrrhotites lie along the FeS–FeS<sub>2</sub> (pyrrhotite–pyrite) binary. The quantitative use of pyrrhotite as a sensor of  $f_{S_2}$  in magmas has been pioneered by Whitney (1984), following the seminal experimental work of Toulmin & Barton (1964). For temperatures above 1000°C, sulphide melts are stable, allowing the interesting

possibility (relative to pyrrhotite) of dissolving significant amount of oxygen (e.g. Kress, 1997), which gives the system an additional degree of freedom from the thermodynamic viewpoint. The implication is that, contrary to common wisdom, a silicic melt saturated in a sulphide has no reason to have its sulphur content buffered to a constant value at fixed  $P$ – $T$ , simply because the sulphide phase has no fixed composition (see also Clemente *et al.*, 2004). The qualitative effects of sulphur on phase relations and compositions can be understood by analogy with that of water

Table 6: Experimental orthopyroxene compositions

| Run no.:                                       | MS29  |       | MS24  |       | PEL2  |       | PEL3  |       |
|--|-------|-------|-------|-------|-------|-------|-------|-------|
| <i>P</i> (GPa):                                | 2     |       | 3     |       | 3     |       | 3     |       |
| <i>T</i> (°C):                                 | 950   |       | 950   |       | 900   |       | 800   |       |
| H <sub>2</sub> O (wt %):                       | 6.5   |       | 7.3   |       | 8.5   |       | 8.5   |       |
| S (wt %):                                      | 2     |       | 2     |       | 4     |       | 4     |       |
| Analyses:                                      | 3     | SD    | 5     | SD    | 7     | SD    | 3     | SD    |
| <i>wt % oxide</i>                              |       |       |       |       |       |       |       |       |
| SiO <sub>2</sub>                               | 52.99 | 0.50  | 51.00 | 0.31  | 52.26 | 0.75  | 54.02 | 0.50  |
| TiO <sub>2</sub>                               | 0.41  | 0.10  | 0.36  | 0.08  | 0.19  | 0.04  | 0.11  | 0.03  |
| Al <sub>2</sub> O <sub>3</sub>                 | 3.14  | 0.26  | 5.70  | 0.27  | 9.09  | 0.48  | 8.34  | 0.40  |
| FeO  | 11.99 | 0.78  | 13.17 | 0.41  | 2.78  | 0.38  | 4.95  | 0.38  |
| MnO  | 0.42  | 0.06  | 0.34  | 0.12  | 0.16  | 0.05  | 0.32  | 0.14  |
| MgO  | 27.58 | 0.65  | 24.38 | 0.45  | 33.76 | 0.44  | 31.86 | 0.20  |
| CaO  | 1.56  | 0.27  | 1.53  | 0.24  | 0.04  | 0.01  | 0.01  | 0.01  |
| Na <sub>2</sub> O                              | 0.02  | 0.02  | 0.10  | 0.06  | 0.04  | 0.02  | 0.02  | 0.01  |
| Total  | 98.12 | 0.62  | 96.59 | 0.78  | 98.31 | 0.59  | 99.62 | 0.13  |
| <i>Structural formula (based on 6 oxygens)</i> |       |       |       |       |       |       |       |       |
| Si   | 1.923 | 0.004 | 1.889 | 0.007 | 1.805 | 0.014 | 1.853 | 0.012 |
| Ti   | 0.011 | 0.003 | 0.010 | 0.002 | 0.005 | 0.001 | 0.003 | 0.001 |
| Al   | 0.135 | 0.012 | 0.249 | 0.012 | 0.370 | 0.021 | 0.337 | 0.016 |
| Fe <sub>tot</sub>                              | 0.364 | 0.026 | 0.408 | 0.012 | 0.080 | 0.011 | 0.142 | 0.011 |
| Mn   | 0.013 | 0.002 | 0.011 | 0.004 | 0.005 | 0.001 | 0.009 | 0.004 |
| Mg   | 1.492 | 0.025 | 1.346 | 0.015 | 1.738 | 0.013 | 1.630 | 0.010 |
| Ca   | 0.061 | 0.010 | 0.061 | 0.010 | 0.001 | 0.000 | 0.000 | 0.000 |
| Na   | 0.002 | 0.001 | 0.007 | 0.004 | 0.003 | 0.001 | 0.001 | 0.001 |
| Mg#  | 0.80  | 0.01  | 0.77  | 0.01  | 0.96  | 0.01  | 0.92  | 0.01  |

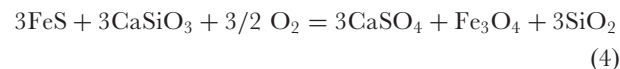
The 'analyses' row refers to the number of analyses used to calculate the average. SD, standard deviation. Mg# = Mg/(Mg + Fe).

on plagioclase in silicate liquids: the more water is added, the more calcic the plagioclase becomes, up to the point when plagioclase is no longer stable, whereupon the liquid is the most calcium- and aluminium-rich possible (for a given bulk composition). For sulphur, the more is added, the more iron is held by sulphide, and, as a result, the more Mg-rich the coexisting liquid and ferro-magnesian silicates. The affinity of sulphur for iron under reducing or moderately reducing conditions is so high that it forces other Fe-bearing phases to become Mg-rich, as observed here for garnet, amphibole or clinopyroxene, and as documented in previous experimental studies (e.g. Popp *et al.*, 1977; Tso *et al.*, 1979; Scaillet & Evans, 1999; Costa *et al.*, 2004; Parat *et al.*, 2008).

### Basaltic system

An increase in the sulphur content in the basaltic system at 3 GPa and 900°C leads to an increase in glass abundance

and a decrease in clinopyroxene abundance (Fig. 4). This has significant consequences for melt compositions, as discussed below. A general reaction that may account for the decrease in clinopyroxene stability in magmas with increasing  $fO_2$  in the presence of sulphur is (Carroll & Rutherford, 1987)



where the sulphur-bearing species may be either solid (pyrrhotite, anhydrite) or liquid phases, and CaSiO<sub>3</sub> is the wollastonite component in clinopyroxene. An increase in  $fO_2$  drives reaction (4) to the right, leading to clinopyroxene consumption and to an increase of S complexed with Ca.

At 3 GPa amphibole is stable at 700 and 800°C in the 2 wt % S experiments, whereas its presence is not documented above 750°C at pressures exceeding 2.5 GPa in

Table 7: *Experimental biotite composition*

|   |       |       |
|---|-------|-------|
| Run no.:  | PEL3  |       |
| $P$ (GPa):                                      | 3     |       |
| $T$ ( $^{\circ}\text{C}$ ):                     | 800   |       |
| $\text{H}_2\text{O}$ (wt %):                    | 8.5   |       |
| S (wt %):                                       | 4     |       |
| Analyses:                                       | 5     | SD    |
| <i>wt % oxide</i>                               |       |       |
| $\text{SiO}_2$                                  | 41.36 | 0.26  |
| $\text{TiO}_2$                                  | 1.89  | 0.08  |
| $\text{Al}_2\text{O}_3$                         | 16.64 | 0.25  |
| FeO   | 3.67  | 0.19  |
| MnO   | 0.03  | 0.04  |
| MgO   | 20.11 | 0.19  |
| CaO   | 0.01  | 0.02  |
| $\text{Na}_2\text{O}$                           | 0.23  | 0.02  |
| $\text{K}_2\text{O}$                            | 9.61  | 0.13  |
| Total   | 93.55 | 0.44  |
| <i>Structural formula (based on 11 oxygens)</i> |       |       |
| Si  | 2.946 | 0.015 |
| Ti  | 0.101 | 0.004 |
| Al  | 1.397 | 0.018 |
| $\text{Fe}_{\text{tot}}$                        | 0.219 | 0.012 |
| Mn  | 0.002 | 0.002 |
| Mg  | 2.136 | 0.020 |
| Ca  | 0.001 | 0.001 |
| Na  | 0.032 | 0.003 |
| K   | 0.873 | 0.012 |
| Mg#   | 0.91  | 0.01  |

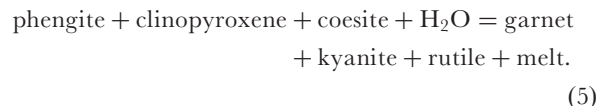
The ‘analyses’ row refers to the number of analyses used to calculate the average. SD, standard deviation.  $\text{Mg\#} = \text{Mg}/(\text{Mg} + \text{Fe})$ .

sulphur-free basaltic systems, even under high  $f\text{O}_2$ , known to promote amphibole stability (Prouteau *et al.*, 2001; Klimm *et al.*, 2008). High Mg# (up to 0.72) amphibole produced in these experiments compares well with amphibole preserved in sulphur-rich silicate melt inclusions in Batan mantle xenoliths (Mg# 0.72–0.82) (Schiano *et al.*, 1995; Métrich *et al.*, 1999). Our experimental results thus suggest that, at high pressure, amphibole stability in basaltic systems is enhanced by high sulphur contents, probably because of the increased Mg# of the liquid.

### Pelitic system

The presence of orthopyroxene instead of garnet in pelite with 4 wt % bulk sulphur at 3 GPa is probably linked to the change in liquid Mg# owing to the addition of high amounts of sulphur in these charges. No phengite was

detected in our experimental charges. Comparison with other studies on the behaviour of S-free pelite or greywacke compositions at high pressures shows that phengite is stable in these compositions at 3 GPa up to at least 900 $^{\circ}\text{C}$  (Alt & Shanks, 2003; Schmidt *et al.*, 2004; Hermann *et al.*, 2006; Hermann & Spandler, 2008), regardless of the composition of the starting material. Although we have not worked out in detail the pelite phase equilibria in the pressure range investigated, we suggest that the lack of phengite is, *inter alia*, due to the higher water contents of our experiments, as compared with other studies (e.g. Hermann & Spandler, 2008). Because our experiments investigated fluid-induced melting of metapelite, the following melting reaction applies (Hermann & Spandler, 2008), in which all the reactant phases have been melted out:



Another possible (but not exclusive) explanation for the lack of phengite is the presence of sulphur. If sulphur indeed affects garnet stability, then its presence in pelite may drive reaction (5) to the right, leading to earlier phengite consumption relative to S-free conditions. However, disentangling the relative roles of  $\text{H}_2\text{O}$  and sulphur in pelite phase equilibria must await further experimental work.

### Sulphur solubilities in hydrous felsic melts at high pressure

Our experiments show that high sulphur solubilities in slab melts are reached by hydrous melting at high  $f\text{O}_2$ , at a pressure higher than 2 GPa, ideally 3 GPa, and with a bulk S content higher than 1 wt % in the source. The main compositional difference between our melts at  $\text{NNO} + 1$  and those obtained at low pressures is the higher water content of the former, which ranges between 12 and 31 wt %, depending on the degree of melting. Previous work has shown that the solubility of sulphate in felsic melts increases when the activity of silica decreases (Ducea *et al.*, 1999). On this basis, we infer that the increase in sulphur we document in our oxidized charges is in part controlled by the very high melt water content achievable in high-pressure silicic melts, which strongly decreases their silica activity (see below). However, the fact that the reduced experiment, which has also a high dissolved  $\text{H}_2\text{O}$  content, does not achieve such a high S content, shows that the enhanced sulphur solubility is also related to speciation effects, as it is well known that  $f\text{O}_2$  affects sulphur speciation and solubility in silicate melts (Carroll & Webster, 1994; Jugo & Luth, 2005).

Table 8: Compositions of experimental glasses (normalized to 100 wt% anhydrous)

| Run no.:                               | MS7         | MS6         | MS26        | MS29        | MS5       | MS1         | MS22        | MS10        | MS9         | MS11        | MS24        | PEL1      | PEL3      | PEL2      |
|--|-------------|-------------|-------------|-------------|-----------|-------------|-------------|-------------|-------------|-------------|-------------|-----------|-----------|-----------|
| <i>P</i> (GPa):                        | 2           | 2           | 2           | 2           | 3         | 3           | 3           | 3           | 3           | 3           | 3           | 3         | 3         | 3         |
| <i>T</i> (°C):                         | 800         | 900         | 900         | 950         | 800       | 900         | 700         | 800         | 900         | 900         | 950         | 900       | 800       | 900       |
| H <sub>2</sub> O <sub>in</sub> (wt %): | 6.7         | 6.6         | 6.0         | 6.5         | 6.2       | 5.4         | 6.8         | 6.6         | 5.4         | 8.1         | 7.3         | -         | -         | -         |
| S <sub>in</sub> (wt %):                | 1           | 1           | 2           | 2           | 1         | 1           | 2           | 2           | 2           | 2           | 2           | 1         | 4         | 4         |
| Log <i>f</i> S <sub>2</sub> :          | 1.68        | 1.72        | 2.1         | 1.85        | 3.56      | 3.44        | 1.50        | 2.37        | 3.06        | -0.89       | 2.83        | 3.57      | 2.80      | 5.46      |
| Capsule:                               | Au          | Au          | Au          | Au          | Au        | Au          | Au          | Au          | Au          | graphite-Pt | Au          | Au        | Au        | Au        |
| <i>n</i> :                             | 6           | 11          | 8           | 14          | 8         | 9           | 6           | 9           | 10          | 11          | 12          | 8         | 8         | 9         |
| SiO <sub>2</sub>                       | 71.59(1.49) | 62.07(1.44) | 63.95(1.05) | 59.41(2.54) | 68.83(84) | 68.44(60)   | 73.13(1.51) | 71.31(1.26) | 67.04(1.21) | 69.14(2.65) | 62.78(3.18) | 75.33(19) | 76.21(37) | 74.84(56) |
| Al <sub>2</sub> O <sub>3</sub>         | 15.13(29)   | 19.58(60)   | 20.27(30)   | 18.06(47)   | 17.45(25) | 17.87(34)   | 15.09(27)   | 17.19(38)   | 17.84(43)   | 17.27(1.32) | 17.21(1.07) | 14.98(16) | 13.81(23) | 15.83(18) |
| FeO <sub>tot</sub>                     | 2.46(36)    | 5.24(1.29)  | 3.18(61)    | 6.59(1.15)  | 0.58(19)  | 1.60(44)    | 1.79(70)    | 1.71(46)    | 2.26(74)    | 2.88(59)    | 5.20(2.00)  | 1.09(12)  | 0.96(12)  | 0.12(9)   |
| MgO                                    | 1.15(38)    | 0.97(57)    | 0.74(24)    | 2.73(93)    | 0.09(10)  | 0.44(18)    | 0.52(53)    | 0.58(14)    | 0.80(38)    | 0.99(19)    | 1.86(1.05)  | 1.20(4)   | 1.62(5)   | 1.97(11)  |
| CaO                                    | 4.10(33)    | 6.76(21)    | 7.17(17)    | 7.99(45)    | 2.63(9)   | 4.03(36)    | 3.63(35)    | 4.89(44)    | 5.38(73)    | 3.87(48)    | 6.38(0.65)  | 0.46(4)   | 0.46(5)   | 0.41(5)   |
| Na <sub>2</sub> O                      | 3.85(16)    | 3.35(40)    | 2.67(36)    | 3.40(53)    | 8.62(75)  | 5.20(52)    | 4.63(44)    | 3.08(1.32)  | 4.01(41)    | 3.31(38)    | 3.51(0.47)  | 3.11(8)   | 2.50(20)  | 2.94(28)  |
| K <sub>2</sub> O                       | 0.91(5)     | 0.59(9)     | 0.58(7)     | 0.44(6)     | 0.96(5)   | 0.99(10)    | 0.85(8)     | 0.59(9)     | 0.85(8)     | 1.05(8)     | 0.76(0.09)  | 3.37(7)   | 4.06(12)  | 3.27(12)  |
| TiO <sub>2</sub>                       | 0.47(6)     | 0.73(17)    | 0.85(16)    | 1.12(21)    | 0.44(12)  | 0.75(17)    | 0.17(8)     | 0.33(15)    | 0.95(13)    | 0.79(8)     | 1.71(0.23)  | 0.35(9)   | 0.25(10)  | 0.49(10)  |
| MnO                                    | 0.14(15)    | 0.14(8)     | 0.13(14)    | 0.22(9)     | 0.05(8)   | 0.07(7)     | 0.09(4)     | 0.06(4)     | 0.24(67)    | 0.09(10)    | 0.08(0.08)  | 0.03(4)   | 0.05(4)   | 0.04(6)   |
| P <sub>2</sub> O <sub>5</sub>          | 0.11(5)     | 0.57(3)     | 0.48(7)     | 0.44(7)     | 0.35(4)   | 0.62(8)     | 0.09(6)     | 0.26(4)     | 0.63(6)     | 0.61(21)    | 0.51(0.05)  | 0.10(2)   | 0.08(2)   | 0.07(5)   |
| Hydrous total                          | 90.14(1.23) | 86.70(74)   | 84.77(61)   | 88.49(0.92) | 90.21(69) | 86.49(1.54) | 87.73(1.22) | 88.37(72)   | 82.99(1.16) | 87.20(70)   | 84.19(1.64) | 89.08(52) | 87.98(87) | 87.04(73) |
| H <sub>2</sub> O <sub>by diff.</sub>   | 7.31(1)     | 11.4(6)     | 12.2(5)     | 8.9(8)      | 8.5(6)    | 10.71(3)    | 9.6(1.1)    | 10.6(7)     | 13.7(1.0)   | 10.1(6)     | 12.6(1.4)   | 9.4(4)    | 10.3(7)   | 10.2(6)   |
| H <sub>2</sub> O <sub>calc.</sub>      | -           | -           | -           | -           | 22.9      | 19.9        | -           | -           | 16.9        | 31.5        | 20.6        | 11.7      | -         | -         |
| S melt (ppm)                           | 289(22)     | 299(56)     | 1509(94)    | 1916(620)   | 92(29)    | 1250(113)   | 570(29)     | 1284(95)    | 4692(377)   | 228(28)     | 5032(427)   | 251(31)   | 2541(81)  | 9767(152) |
| <i>r</i> (S)                           | 7           | 11          | 12          | 19          | 9         | 7           | 4           | 8           | 15          | 4           | 18          | 6         | 11        | 14        |
| X <sub>Mg</sub>                        | 0.46        | 0.25        | 0.29        | 0.43        | 0.21      | 0.33        | 0.34        | 0.38        | 0.39        | 0.26        | 0.39        | 0.66      | 0.75      | 0.97      |
| A/CNK                                  | 1.05        | 1.06        | 1.12        | 0.91        | 0.87      | 1.05        | 1.00        | 1.18        | 1.03        | 1.27        | 0.95        | 1.56      | 1.48      | 1.73      |
| Ab%                                    | 54.56       | 43.36       | 36.70       | 41.65       | 79.55     | 63.01       | 62.97       | 48.43       | 51.66       | 52.48       | 45.12       | 54.47     | 44.66     | 53.83     |
| An%                                    | 35.98       | 51.33       | 57.73       | 54.61       | 14.26     | 28.64       | 28.96       | 45.09       | 40.71       | 35.91       | 48.09       | 4.68      | 4.77      | 4.44      |
| Or%                                    | 9.46        | 5.32        | 5.57        | 3.74        | 6.19      | 8.35        | 8.07        | 6.48        | 7.63        | 11.61       | 6.79        | 40.85     | 50.57     | 41.74     |

H<sub>2</sub>O<sub>in</sub> and S<sub>in</sub> represent the amounts of water and sulphur loaded to the capsule. H<sub>2</sub>O determined by using the by-difference (H<sub>2</sub>O<sub>by diff.</sub>) method or using mass-balance constraints (H<sub>2</sub>O<sub>calc.</sub>) and assuming perfectly incompatible behaviour of K<sub>2</sub>O for charges not having either amphibole or biotite. The log *f*S<sub>2</sub> is calculated using the method of Bockrath *et al.* (2004) as modified by Liu *et al.* (2007).

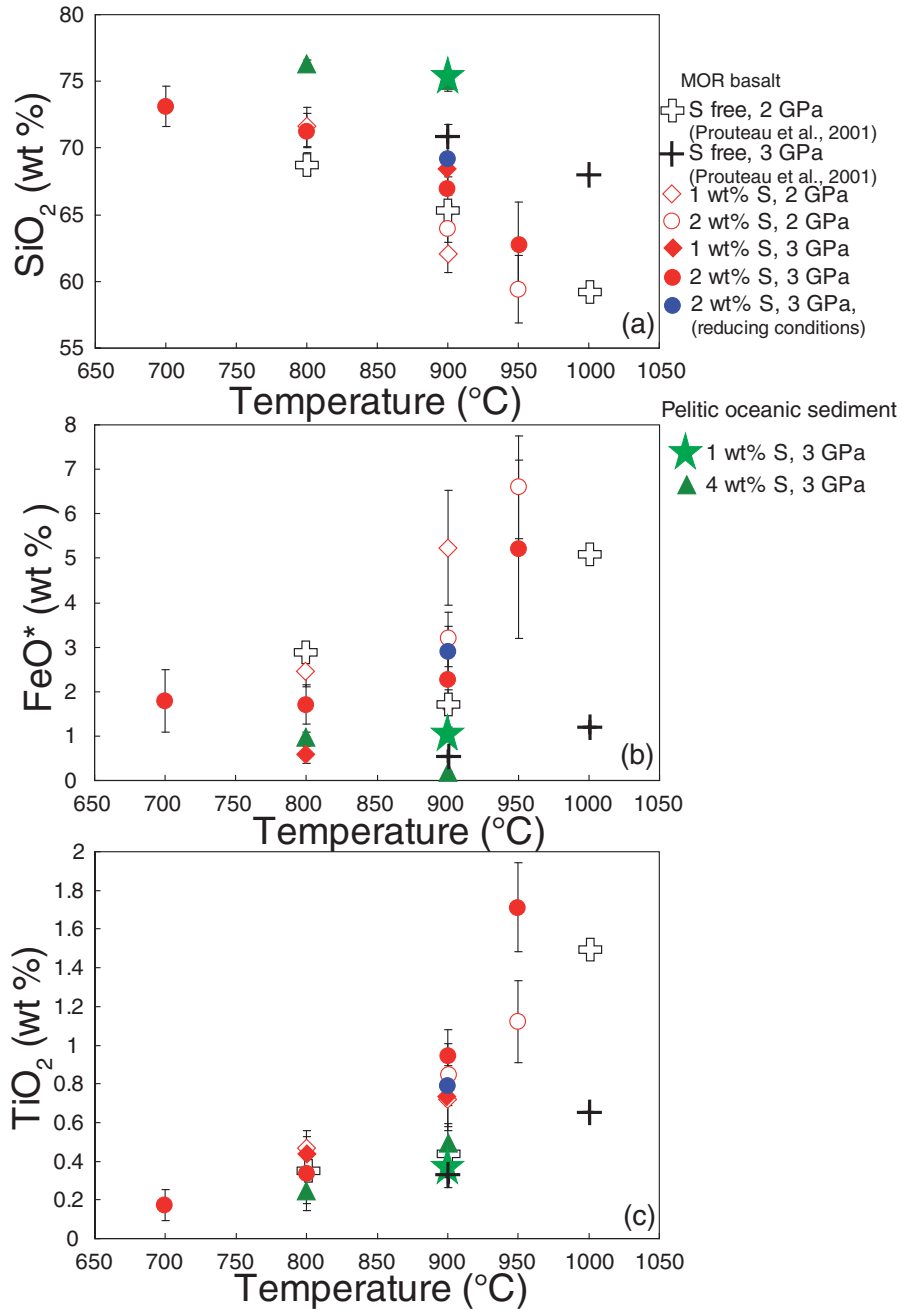
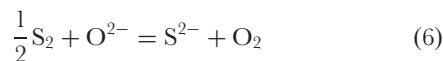
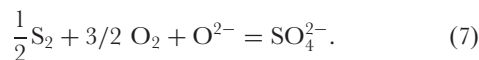


**Fig. 8.** Variation of melt composition with temperature: (a) SiO<sub>2</sub>; (b) FeO\*(total); (c) TiO<sub>2</sub>. Data from this study and Prouteau *et al.* (2001).

The usual proposed dissolution reaction of sulphur in anhydrous silicate melts can be written as (Carroll & Webster, 1994)



for sulphide, whereas for sulphate it is



Several experimental investigations have indeed confirmed that these two reactions readily account for the systematics of sulphur dissolution and solubility in a variety of silicate melts (e.g. Carroll & Webster, 1994; O'Neill & Mavrogenes, 2002; Jugo *et al.*, 2005), most notably in those that are dry and mafic. The O<sup>2-</sup> species represent non-bridging oxygens (i.e. not linked with Al or Si cations that build the tetrahedral framework), for which S<sup>2-</sup> substitutes in the silicate melt. The strong correlation between iron content and amount of sulphur dissolved in

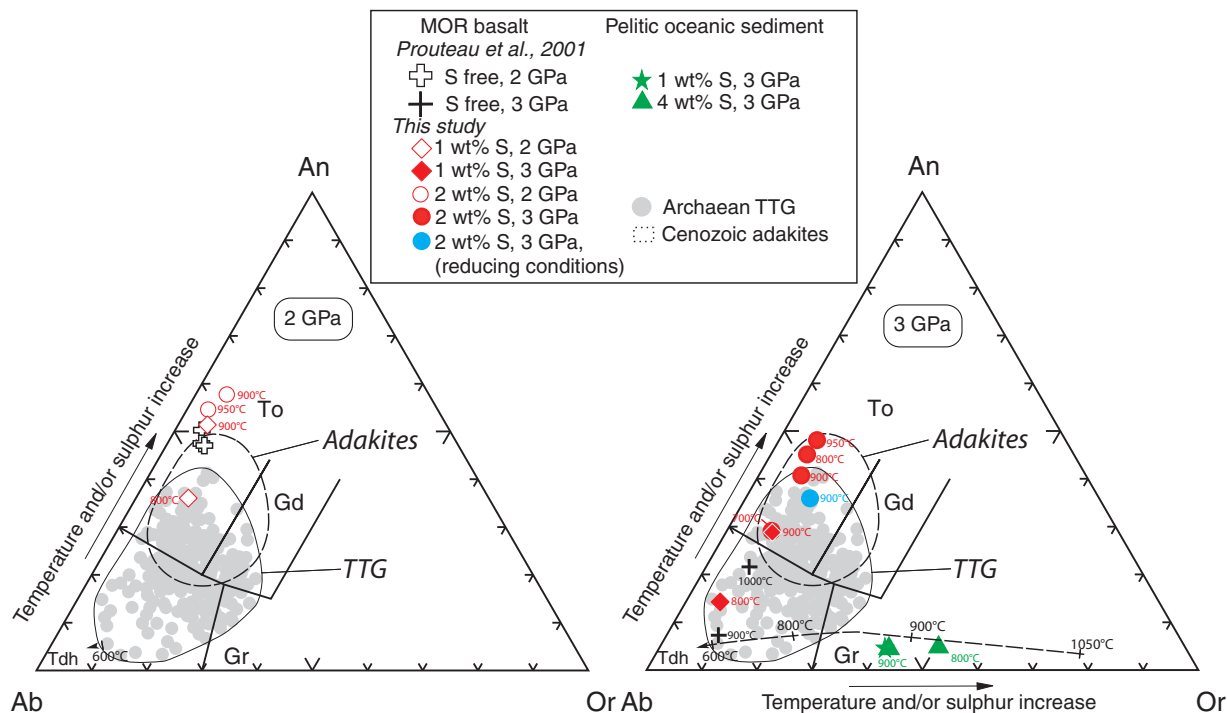


**Fig. 9.** Anorthite–albite–orthoclase normative triangle showing the experimental glass compositions with (this study) and without sulphur (Prouteau *et al.*, 2001; Hermann & Spandler, 2008), at 2 and 3 GPa (left and right panels, respectively). Also shown are fields for Archean granitoids (TTG) (Martin, 2005) and Phanerozoic slab melts (adakites) (Defant & Drummond, 1990). All but one S-bearing experiment produced liquids falling in the tonalite field, where most adakites plot. In contrast, at 3 GPa, partial melting of a hydrous- and sulphur-free basalt at temperatures at or below 1000°C (Prouteau *et al.*, 2001) yields liquids within the trondhjemite field only (black crosses), which characterizes a large fraction of the TTG suite, notably in the early Archean (Martin, 2005). The dashed line with ticks represents the evolution with temperature of silicate melts ( $\geq 800^\circ\text{C}$ ) or fluids ( $< 800^\circ\text{C}$ ) produced from partial melting of hydrous pelite without sulphur (Hermann & Spandler, 2008). (Note in particular the large compositional difference observed at  $800^\circ\text{C}$  between sediment melts with and without sulphur). Colour coded experimental temperatures are shown close to either symbols or ticks. Those corresponding to Prouteau *et al.* (2001) at 2 GPa (800–1000°C) have been omitted for clarity. To, tonalite; Tdh, trondhjemite; Gd, granodiorite; Gr, granite.

both natural and experimental liquids suggests that such free oxygens are primarily those complexed with divalent iron (Carroll & Webster, 1994; O'Neill & Mavrogenes, 2002; Jugo *et al.*, 2005). For sulphate, the case has been made that Ca is the main divalent element associated with the free oxygen at high  $f\text{O}_2$  (Carroll & Webster, 1994; Mavrogenes & O'Neill, 1999; Jugo *et al.*, 2005).

A number of solubility models for magmas saturated in sulphide have been derived, based on standard thermodynamic formulations for the above reactions (Mavrogenes & O'Neill, 1999; Holzheid & Groves, 2002; O'Neill & Mavrogenes, 2002; Liu *et al.*, 2007; Moretti & Baker, 2008). The most recent of such models takes explicitly into account the effect of water (Liu *et al.*, 2007) and is calibrated on basaltic to silicic melt compositions, with dissolved water contents of up to 9 wt %. The role of  $f\text{O}_2$  is incorporated indirectly, via the use of the iron redox ratio as model input. Application of the Liu *et al.* (2007) model to our melts, most of which are sulphide-saturated (Table 2), is shown in Fig. 12, using an average  $f\text{O}_2$  of NNO +1 (or

NNO – 2 for the reduced charge) to calculate the iron redox state (Kress & Carmichael, 1991). Clearly, this model (and any other one based on the same premise that iron is the main parameter in controlling sulphur solubilities) falls short in calculating the measured sulphur contents of our hydrous silicic melts; the difference between observed and calculated S contents is in general about two, in some cases more than three, orders of magnitude. The magnitude of the discrepancy cannot be due to a poor evaluation of any input parameter in the model equation of Liu *et al.* (2007), which are essentially compositional or first-order intensive parameters ( $P$  and  $T$ ), all of which are well known in our experiments. Rather, this suggests that the postulated dissolution mechanisms on which the modelling approach is based might not hold for  $\text{H}_2\text{O}$ -rich, Fe-poor and oxidized liquids.

An alternative approach to understand sulphur solubility in hydrous melts was taken by Burnham (1979) on the basis of sulphur solubility experiments in hydrous albitic liquids (thus iron poor). Burnham (1979) proposed that

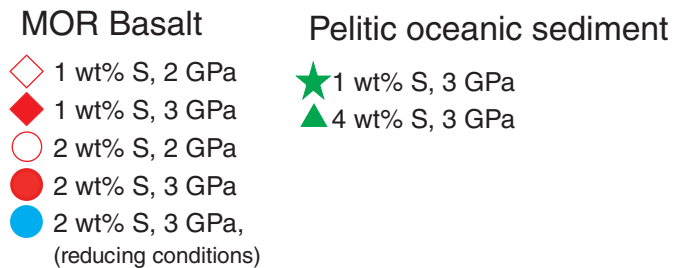
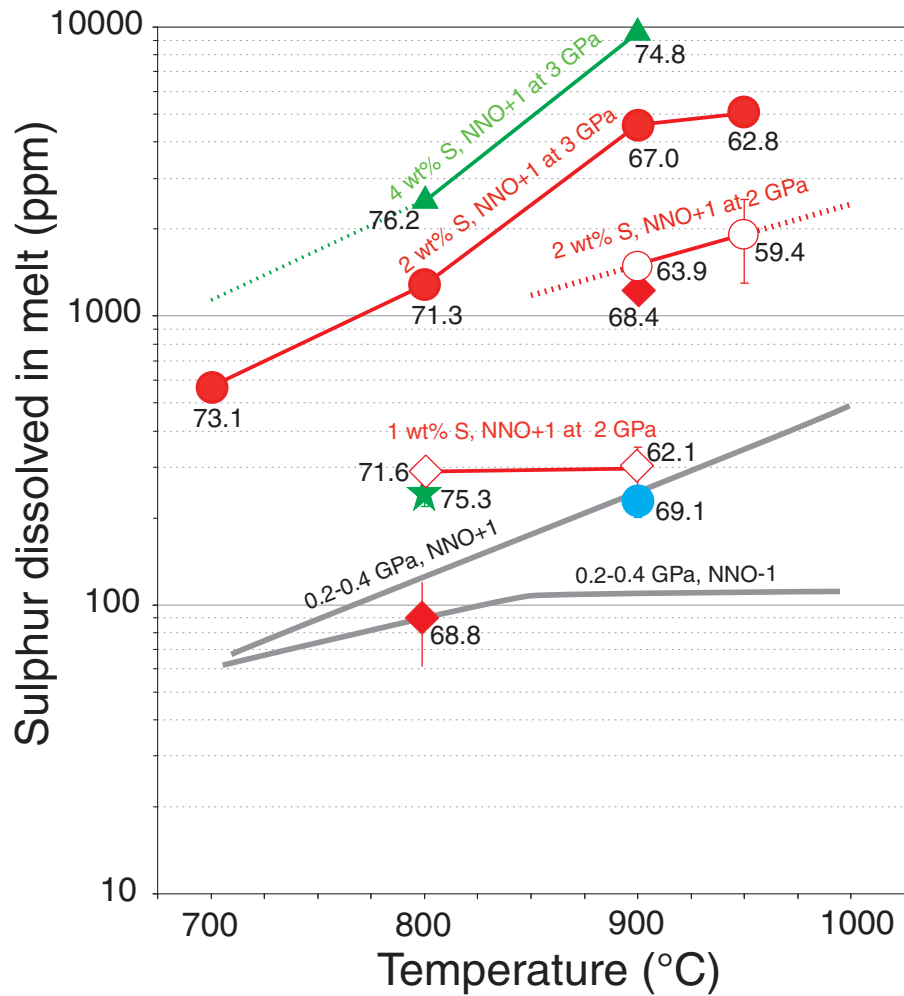
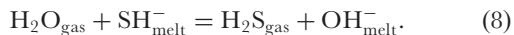


**Fig. 10.** Sulphur contents (ppm) of experimental glasses as a function of temperature. Vertical bars are  $1\sigma$  standard deviations (when not shown error bars are smaller than the symbol size). Dashed lines are extrapolated experimental trends. The blue dot shows the charge annealed at around NNO - 2 using a capsule lined with graphite. All other colored symbols (red for basalt and green for pelite) represent experiments performed at around NNO + 1. The two grey lines show the sulphur content of silicic melts at 0.2-0.4 GPa saturated in either sulphide or sulphate at two different  $fO_2$  values, NNO + 1 and NNO - 1 (referenced relative to the Ni-NiO solid buffer, in log units), based on available experimental data (Luhr, 1990; Carroll & Webster, 1994; Scaillet *et al.*, 1998; Wallace, 2005). For clarity, experiments at 0.2-0.4 GPa carried out at an  $fO_2$  of NNO + 3 or above are not shown, as we currently lack equivalent runs on silicic melts at 2-3 GPa. The overall positive trends reflect the increase in  $fS_2$  and the additive roles of temperature (Carroll & Webster, 1994) and decreasing silica content (Ducea *et al.*, 1999) (labelled along the curves), both of which increase the sulphur content of the silicate melt, everything else being equal (Fig. 2).

sulphur species are essentially in a substitution reaction with water species dissolved in the liquid such as



For  $\text{SO}_2$ , Clemente *et al.* (2004) suggested the following reaction:



Although the exact nature of the involved species (e.g. hydroxyl or molecular water) can be debated, the above reactions show that the addition of hydrogen leads to the incoming of  $\text{H}_2\text{S}$  in addition to  $\text{SO}_2$  and  $\text{S}_2$  species, and that water species may offer alternative opportunities for sulphur dissolution sites in silicate melts, in addition to complexation reactions with dissolved iron. The occurrence of  $\text{HS}^-$  in Fe-poor, hydrous, reduced silicate melts has recently been documented by Klimm & Botcharnikov (2010), using Raman spectroscopy, lending support to Burnham's original suggestion. Clemente *et al.* (2004) used an extensive set of hydrous experiments with controlled  $f\text{O}_2$  and  $f\text{S}_2$  to propose a thermodynamic model of sulphur solubility in hydrous silicic melts, in which the sulphur content is controlled by the fugacities of both  $\text{H}_2\text{S}$  and  $\text{SO}_2$  species (and thus the dissolution of the corresponding species), depending on the prevailing  $f\text{O}_2$ . Such a model, although successfully reproducing the experimental data, also illustrates that iron is not mandatory to achieve elevated sulphur contents in silicate liquids (Burnham, 1979; Clemente *et al.*, 2004; Klimm & Botcharnikov, 2010). In our charges, the relatively high  $f\text{S}_2$ , along with elevated  $f\text{O}_2$ , implies that high  $f\text{SO}_2$  prevails in oxidized runs (or  $f\text{H}_2\text{S}$  in reduced runs). Application of the thermodynamic model of Clemente *et al.* (2004) to our  $P$ - $T$ - $f\text{O}_2$ - $f\text{S}_2$ - $f\text{H}_2\text{O}$  conditions (Fig. 13) shows that such an approach has no particular problems in generating high sulphur contents in hydrous and low-temperature silicate liquids at  $f\text{O}_2$  higher than NNO. For instance, at NNO +1 and  $\log f\text{S}_2 = 4$ , a silicic melt reaches a sulphur content of *c.* 6000 ppm (Fig. 13), which is within the order of magnitude of our experimental observations (Table 8, Fig. 10). In the low  $f\text{O}_2$  range, predicted sulphur contents are much lower, also in agreement with experimental data. Thus, despite the fact that the model is being used well outside the calibrated range, it rather successfully predicts experimental observations, unlike other modelling approaches using iron sulphur complexes as a central concept. The differences in sulphur contents between calculated and observed values are for most charges within a factor of 2–4 of each other (i.e. observed values are higher than calculated values). We suggest that this is in part due to the effect of  $\text{H}_2\text{O}$  on the silica activity ( $a_{\text{SiO}_2}$ ), an effect not taken into account in the model of Clemente *et al.* (2004).

Experiments by Ducea *et al.* (1999) have indeed shown that, under oxidizing conditions, felsic but silica-poor (i.e. nepheline normative) liquids dissolve 2–4 times more sulphur than their silicic counterpart. Similarly, experiments on dry basalts at 1 GPa at 1300–1350°C under various  $f\text{O}_2$  conditions indicate that sulphate is stable at lower  $f\text{O}_2$  as compared with silicic melts, suggesting that decreasing  $a_{\text{SiO}_2}$  shifts the sulphide or sulphate boundary in silicate melts (e.g. Jugo *et al.*, 2005). This is qualitatively predicted by equilibrium (4), which is driven to the right when  $a_{\text{SiO}_2}$  decreases. The Jugo *et al.* (2005) experiments also show that the sulphur content in sulphate-saturated dry basalt under these conditions exceeds 1 wt %, or 10 times more than at low  $f\text{O}_2$ . It is worth stressing that our experiments at high  $f\text{O}_2$  achieve sulphur contents comparable with those of dry basalt at 1 GPa, but they do so at temperatures 400°C lower, therefore outlining the instrumental role of water in enhancing sulphur dissolution in low-temperature oxidized silicic melts at high pressure. A recent study of sulphur solubility in iron-rich hydrous basalts and andesites also suggests that water has a positive role in increasing sulphur solubilities (Moune *et al.*, 2009).

Based on the above lines of evidence, we conclude that in hydrous silicic melts, sulphur dissolution mechanisms primarily involve interaction with dissolved water species, as Burnham (1979) originally suggested, and, everything else being equal, the sulphur content of hydrous melts is bound to increase with increasing melt water content. The elevated  $\text{H}_2\text{O}$  content of silicic slab melts lowers their silica activity, which drives the sulphide or sulphate boundary toward lower  $f\text{O}_2$ , allowing in turn high-pressure hydrous silicic melts to dissolve more sulphur than at lower pressures but comparable  $f\text{O}_2$ . Therefore, the key to high S-solubility is sulphur dissolved as sulphate rather than as sulphide species.

### Effect of sulphur on the composition of slab melts

A number of petrological and geochemical studies have shown that melting of the oceanic crust was an essential mechanism for continental crust production in the Archean (Martin, 2005) and probably still occurs under certain circumstances in the modern Earth, producing silicic melts termed adakites (Defant & Drummond, 1990). Cenozoic adakites are tonalitic magmas (Fig. 9) characterized by a strong depletion in heavy rare earth elements (HREE), which has been taken as evidence for the presence of garnet in the melting residue (Defant & Drummond, 1990). Previous experimental studies have shown that hydrous partial melting of basalt in the eclogite field ( $P > 2.5$  GPa) at temperatures  $< 1000^\circ\text{C}$  produces trondhjemitic melts with very high contents of alkalis, especially  $\text{Na}_2\text{O}$ , and low contents of MgO and FeO (e.g. Rapp & Watson, 1995; Winther, 1996; Rapp *et al.*, 1999; Prouteau *et al.*, 2001; Klimm *et al.*, 2008). Our results show that



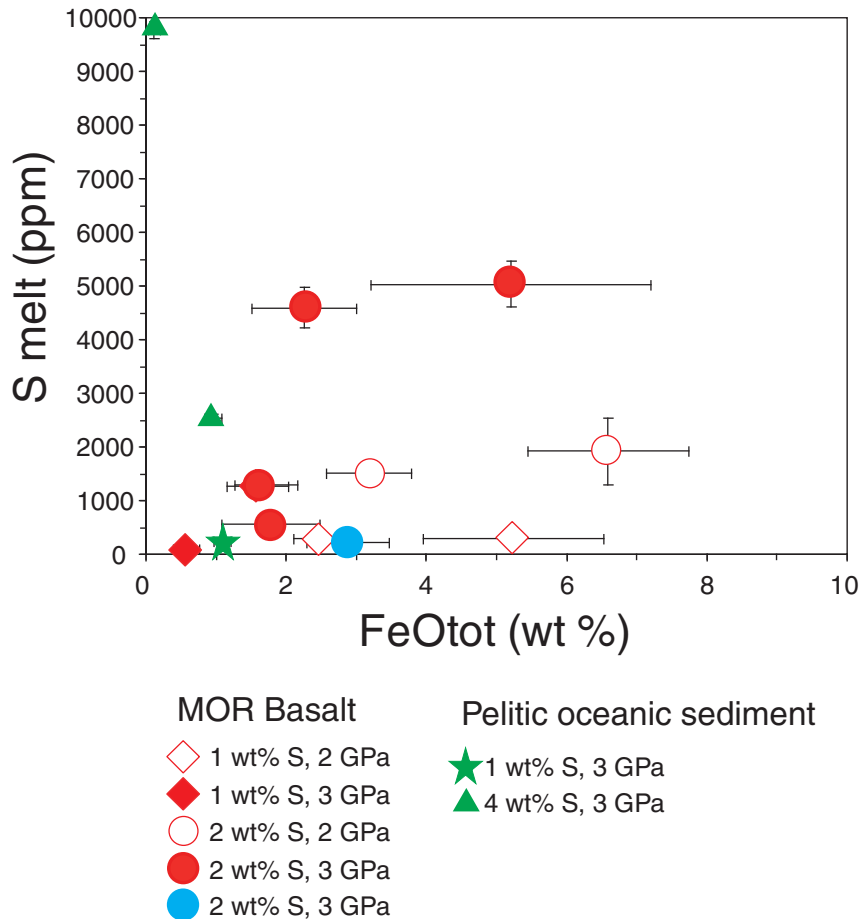


**Fig. 11.** Melt sulphur content versus melt FeO content. (See text for further discussion.)

addition of sulphur to the basalt–H<sub>2</sub>O system produces, for the same  $P$ – $T$ –H<sub>2</sub>O conditions, tonalitic melts with progressive enrichment in anorthite parallel to the albite–anorthite join (Fig. 9), while maintaining an eclogitic mineral assemblage in the residue that fulfils the HREE depletion criterion diagnostic of slab melts. This compositional evolution is explained by the decrease in clinopyroxene modal abundance and glass fraction increase (Fig. 4). Enhanced stability of amphibole in sulphur-rich systems probably also partly explains this evolution. In the S-free system, the increase in the sodic character of residual liquids with pressure is related to the breakdown of amphibole beyond 2 GPa, resulting in the release of all its Na<sub>2</sub>O to the liquid (Prouteau *et al.*, 2001). Altogether, the S-bearing melts are richer in mafic components (CaO, FeO, MgO, TiO<sub>2</sub>) than those produced in sulphur-free charges under the same conditions (Fig. 8). This more mafic character reflects the significant effect of sulphur on phase assemblages and proportions, decreasing the abundances of both pyroxene and garnet (Fig. 4). It is worth pointing out that, in general, the more mafic character of

adakites relative to Archean slab melts is generally attributed to their greater interaction with mantle rocks (Martin, 2005). However, the experimental interaction of slab melts with ultramafic material has been invariably shown to increase both the MgO and Na<sub>2</sub>O content of silicic melts, whereas their CaO content remains broadly constant (Sekine & Wyllie, 1983; Carroll & Wyllie, 1989; Kelemen, 1995; Senn & Dunn, 1995; Rapp *et al.*, 1999; Prouteau *et al.*, 2001); that is, it increases the trondhjemitic character of slab melts. Thus the displacement toward the tonalite field of adakites cannot be attributed to mantle interaction alone. Tonalitic melts derived from partial melting of hydrous basalt can be produced at pressures lower than 2 GPa, but they are in general too Al<sub>2</sub>O<sub>3</sub>-rich (19–21 wt %) compared with adakites (<18 wt %), and do not always coexist with garnet, the key mineral for producing the strong depletion in HREE (Defant & Drummond, 1990; Rapp & Watson, 1995; Rapp *et al.*, 1999; Prouteau *et al.*, 2001; Martin, 2005; Nair & Chacko, 2008). On the basis of this evidence we suggest that the tonalitic character of adakites may witness the enhanced melting

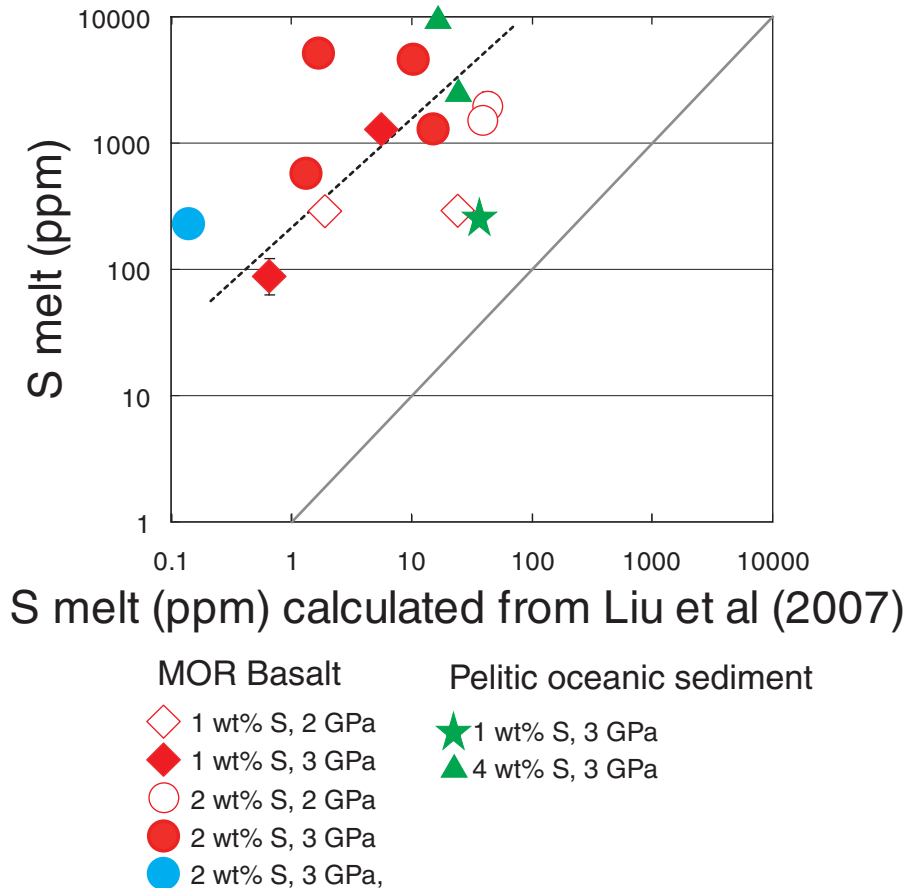


**Fig. 12.** Calculated melt sulphur contents using the model of Liu *et al.* (2007) versus those observed in our quenched glasses. It should be noted that the model of Liu *et al.* (2007) underestimates actual sulphur contents by two orders of magnitude in general. (See text for additional details.)

of localized portions of subducted crust with elevated sulphur contents. An important consequence of our experimental observations is the fact that melting degree increases with sulphur (Fig. 4), which is indicative of the flushing role of this element at high pressure; in other words, the presence of sulphur in hydrous systems at high pressure leads to a depression of solidus temperatures. Owing to the very steep  $dP/dT$  slopes of the solidus of the oceanic crust at high pressure (e.g. Nichols *et al.*, 1994), this may have a significant effect on the pressure of melting and its extent relative to portions of crust devoid of sulphur.

The composition of pelite-derived melts also deserves close scrutiny. One of their most remarkable features is their elevated MgO content, with  $X_{\text{Mg}}$  ranging from 0.66 to 0.97, a feature shared by modern slab melts (Defant & Drummond, 1990) and widely believed to reflect mantle interaction (Sekine & Wyllie, 1983; Carroll & Wyllie, 1989; Kelemen, 1995; Sen & Dunn, 1995; Rapp *et al.*, 1999; Prouteau *et al.*, 2001). Our results suggest that mixing of sulphur-rich pelite-derived melts with those from basalt may also contribute to the production of such slab melts

with a low FeO/MgO ratio, although an increase in MgO from mantle contamination is certainly an important factor in modern arcs. The recent finding of some rare, pristine, high-silica adakites of Miocene age with elevated MgO contents in the Trans-Mexican Volcanic Belt by Gomez-Tuena *et al.* (2008) provides support for such a hypothesis. A second remarkable feature is the lack of phengite in pelitic charges, which drives the residual liquid compositions towards the granitic field, in particular at low temperatures (800°C, Fig. 9). Although it is unclear whether this arises from the effect of either water or sulphur, or from both, comparison with other studies (e.g. Hermann & Spandler, 2008) shows that the first melt generated from an S-free and slightly H<sub>2</sub>O-poor pelite at 600–800°C is strongly trondhjemitic, a result of the buffering role of phengite on residual melt compositions [Fig. 9, Hermann & Spandler (2008); but see Schmidt *et al.* (2004)]. Infiltration of such fluids or melts into the overlying mantle will thus impart a sodic character to the metasomatized mantle. In contrast, melts produced upon phengite breakdown (Schmidt, 1996) will impart a potassic

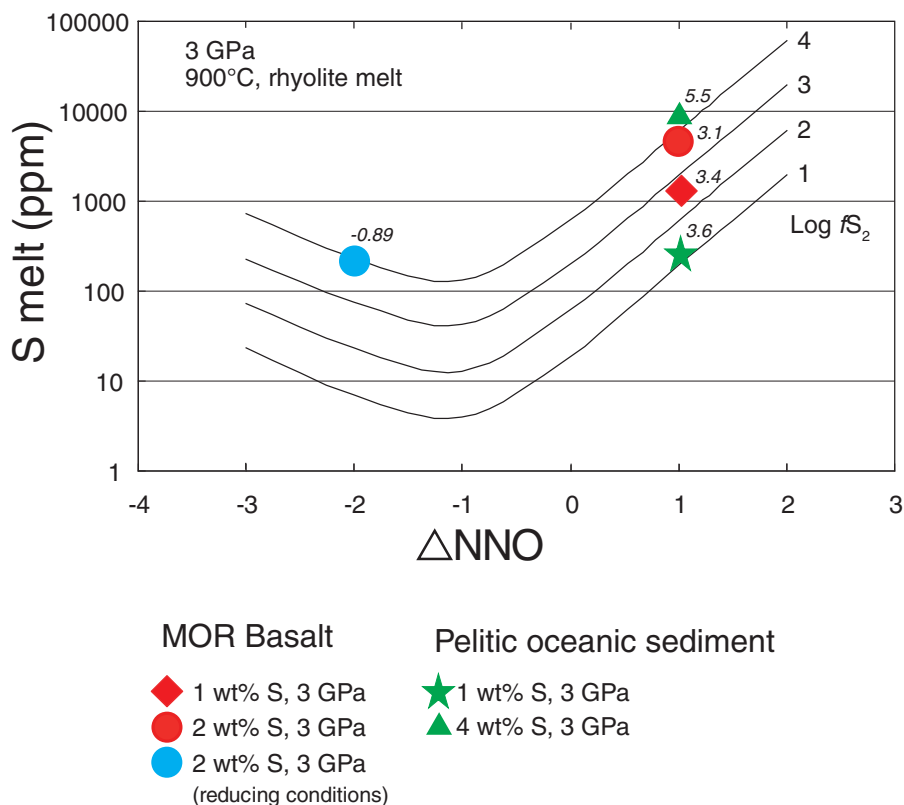


**Fig. 13.** Calculated sulphur content of a rhyolitic melt at 900°C, 3 GPa, and various  $fO_2$  and  $fS_2$ , for a melt water content of 20 wt %. Calculations were performed using the sulphur solubility model of Clemente *et al.* (2004) to relate  $fH_2S$  and  $fSO_2$  to melt sulphur content, and the model of Zhang (1999) to relate  $fH_2O$  to melt water content. (See text for additional details.) Also plotted are the sulphur contents of our experimental melts at 900°C at the inferred  $fO_2$  of synthesis. Numbers next to symbols give the calculated  $fS_2$  with the method of Bockrath *et al.* (2004) as modified by Liu *et al.* (2007). It should be noted that for the reduced charge the indicated  $fS_2$  is the maximum possible one, as  $fO_2$  in the graphite-bearing charge is constrained to be at or below  $NNO - 2$ .

overprint to the sub-arc mantle [note that carbonate–pelite melting also produces strongly potassic liquids (Thomsen & Schmidt, 2008; Spandler *et al.*, 2010; Tsuno & Dasgupta, 2011)]. The conditions at which phengite breaks down are thus critical for determining the Na/K ratio of the fluid or melt infiltrating the mantle, as amply shown by previous experimental studies (e.g. Hermann & Spandler, 2008). Previous studies have mostly emphasized the role of  $P$  and  $T$ . Our results show that  $H_2O$  and sulphur contents may be additional contributing factors. Melts derived from sediments rich in water and sulphur have a distinct K- and S-rich signature, with S/K<sub>2</sub>O (wt %) ratios ranging from 0.007 to 0.3 (Table 8), which compares well with the range found in alkali-rich primitive basalts generated in subduction zones (0.05–0.3) (Métrich & Clochiatti, 1996; Johnson *et al.*, 2009).

Altogether, the significant overlap between adakites and our sulphur-bearing melts provides evidence for the presence of sulphur in Phanerozoic subduction zones, at least in those loci where melting of oceanic crust takes place. Our results also suggest that arc basalts may inherit their

potassium-rich character from a mantle source metasomatized by hydrous partial melts derived dominantly from the top part of the downgoing slab rich in both water and sulphur.

### Implications for the Archean

Our results can now be viewed in the context of current geodynamics and petrogenetic models for arc magmas during the Archean, to evaluate whether sulphur recycling in Precambrian times via subduction zones was as efficient as at present. Archean granitoids (80% of exposed Archean formations), the so-called trondhjemite–tonalite–granodiorite (TTG) series (Martin, 2005; Condie, 2008), are interpreted to be melting products of hydrated basalt protoliths (van der Laan & Wyllie, 1992; de Wit, 1998; Smithies, 2000; Martin, 2005) from either a slab melting process (Martin, 2005) or tectonic stacking of oceanic crust (de Wit, 1998; Smithies, 2000). The common view is that a hotter geothermal gradient prevailed during TTG production, with shallow slab melting (around 1 GPa; Martin, 2005). Our results show that, up to 2 GPa, the

solubility of sulphur in slab melts remains low, hence shallow (<2 GPa) partial melting of oceanic crust would remove a small fraction of its sulphur content, and the majority would remain locked in residual sulphides or sulphates. There is, however, evidence to suggest that conditions for slab melting similar to those of today were reached in at least some Archean convergence zones (Hopkins *et al.*, 2008), which implies deep melting of oceanic crust. A recent experimental investigation has also concluded that the minimum pressure for basalt melting during the Archean is 1.5 GPa, or even 1.8 GPa if plagioclase is not in the residue (Nair & Chacko, 2008). As discussed above, our melt compositions show that deep slab melting with sulphur more probably produces tonalite, not trondhjemite (Fig. 9). Trondhjemite production from slab melting requires both high pressure (e.g. Winther, 1996; Prouteau *et al.* 2001) and sulphur-poor conditions. Hence, because the sulphur-rich character of the modern oceanic crust is acquired via hydrothermal interaction with sulphate-rich seawater (Alt & Shanks, 2003), we suggest that the occurrence of Archean trondhjemites is in agreement with a sulphur-poor ocean as inferred from Archean sedimentary pyrite isotope systematics (Habicht *et al.*, 2002), which suggests sulphate levels in the open ocean *c.* 1% of present-day concentrations. The paucity of volcanogenic massive sulphide deposits (VHMS) prior to 2.5 Ga (Bekker *et al.*, 2010; Huston *et al.*, 2010) is also consistent with a sulphur-poor Archean ocean (Farquhar *et al.*, 2010; Lyons & Gill, 2010). Similarly, the abundance of iron-rich sedimentary formations [so-called banded iron formations (BIF) *sensu lato*] during the Archean suggests that the water columns from which those sediments formed were poor in dissolved sulphur (Lyons & Gill, 2010); however, the interconnections between VHMS and BIF are still unclear (Bekker *et al.*, 2010).

The hypotheses advocated above suggest that the magmatic sulphur return flux via subduction to the Archean continental crust and atmosphere was much lower than that observed today, perhaps by a factor of 100. We note that, because low  $fO_2$  decreases melt sulphur contents (Fig. 10), one could also argue that a low return flux of sulphur reflects that Archean subduction zones were more reduced than today. We do not favour such an interpretation because current views on the evolution of the lithospheric mantle redox state call for limited changes in its  $fO_2$  back to Archean times (Canil, 2002; Li & Lee, 2005). The low sulphate ocean scenario evidenced by the isotopic record (Habicht *et al.*, 2002) is thought to reflect the strongly anoxic character of the Archean atmosphere (Holland, 2002; Farquhar *et al.*, 2007), which would have severely limited the oxidative weathering of continental sulphides and their subsequent delivery to the oceans through river runoff (Holland, 2002). In the light of our results, we suggest that, additionally, the low sulphur content

of the Archean ocean also reflects the fact that the volcanogenic source of atmospheric sulphur was much weaker than during the Phanerozoic. A sulphur-poor TTG source and/or  $P$ – $T$  conditions of TTG production less prone to sulphur transfer both imply that the TTG constructs of the Archean continental crust exposed to surficial weathering must have been poorer in sulphides relative to their modern equivalents. This would have exacerbated the deficit of sulphate produced by any, even limited, oxidative weathering of surface sulphides during the Archean, as opposed to during Proterozoic or Phanerozoic times.

Altogether, the results of our study provide support for the model that, during the Archean, little sulphur was recycled back to the atmosphere via subduction (Holland, 2002, 2009; Farquhar *et al.*, 2010), in sharp contrast to the massive sulphur transfer observed in this geodynamic setting today (Jambon, 1994; Métrich *et al.*, 1999; Wallace, 2005). The main parameters controlling sulphur behaviour appear to be the redox state of both oceanic and atmospheric reservoirs, in addition to subduction style. During the Archean, the transfer of sulphur from the oceanic crust to the mantle wedge appears to have been limited, with S mostly conveyed to the deep mantle during subduction. Conversely, when the ocean and atmosphere reservoirs switched towards oxidizing conditions, and when a colder thermal regime favoured steeper subduction on a global scale, a significant part of the downgoing sulphur was allowed to return to the crust or atmosphere via arc magmatism, as observed today (Jambon, 1994; Wallace, 2005). A related question is thus why did the  $fO_2$  in those reservoirs rise? The answer to this fundamental issue is beyond the scope of the present work but we note that our findings have implications for models giving a pivotal role to the redox state of volcanic gases (Holland, 2002, 2009; Catling & Claire, 2005; Gaillard *et al.*, 2011). In particular, it has been proposed that the abrupt atmospheric rise of  $O_2$  is related to the onset of subaerial arc volcanoes whose gases are on average more oxidized than those of submarine eruptions (Kump & Barley, 2007; Gaillard *et al.*, 2011). Such a shift has been tied to a net increase of high-standing continental landmasses by the end of the Archean, which allowed the establishment of modern, predominantly subaerial, arc-type volcanism. Within this context, we speculate that, in addition to this geomorphological evolution, the increase in sulphur of volcanic gases altered their oxygen consumption potential, which contributed directly to the increase in the redox state of the atmosphere (Holland, 2002, 2009; Gaillard *et al.*, 2011).

## CONCLUSIONS

Our study shows that the sulphur content of high-pressure, oxidized, silicic melts is at least 10–20 times higher than at low pressures. Thus elevated sulphur contents can be achieved in slab melts. This in turn suggests that

Phanerozoic arc magmas may largely owe their sulphur content to slab melt contributions. Such a possibility has been generally dismissed (e.g. De Hoog *et al.*, 2001), essentially because of the low S content of silicic melts obtained in low-temperature and low-pressure experimental studies. Our results remove this apparent limitation, although they do not rule out a fluid contribution for sulphur (whenever the system is below the second critical end point). They also suggest that high concentrations of sulphur may be reached, at least locally, in subducted slabs. The increase of degree of melting with sulphur content (Fig. 4) shows that sulphur triggers partial melting earlier (i.e. at lower temperature) relative to water-only conditions. We thus suggest that melting of subducted slabs occurs preferentially in places where sulphur is present in abundance. Moreover, experimental melts compare well with Phanerozoic slab magmas (adakites), suggesting that sulphur is present in abundance at the locus of slab melting in modern subduction zones. In contrast, the effect of sulphur on melt composition shows that, if melting conditions in Archean subduction zones were similar to those of the present day, then the sodic character of Archean granitoids provides evidence for a sulphur-poor source, in agreement with a sulphate-poor Archean ocean (Habicht *et al.*, 2002; Farquhar *et al.*, 2010). The volcanic output of sulphur during the Archean was possibly much weaker than during Proterozoic–Phanerozoic times, which may have helped to maintain the strongly anoxic condition of the Archean atmosphere. Altogether, our results show that the volcanic contribution to the evolution of Earth's atmosphere–hydrosphere may have varied significantly in style and composition with time and not only in magnitude and strength, as widely assumed.

## ACKNOWLEDGEMENTS

We thank Michel Pichavant, Catherine Chauvel, Fabrice Gaillard, and Clive Oppenheimer for continuous support and fruitful discussions. The paper greatly benefited from constructive reviews by Kevin Klimm and John Mavrogenes, as well as an anonymous reviewer, and the careful editorial handling of Jörg Hermann.

## FUNDING

This project was financially supported by the French ANR funding agency (project UD Antilles) and INSU-CNRS grants.

## REFERENCES

- Alt, J. C. & Burdett, J. W. (1992). Sulfur in Pacific deep-sea sediments (Leg 129) and implications for cycling of sediment in subduction zones. In: Larson, R. L. & Lancelot, Y. *et al.* (eds) *Proceedings of the Ocean Drilling Program, Scientific Results 129*. College Station, TX: Ocean Drilling Program, pp. 283–294.
- Alt, J. C. & Shanks, W. C. (2003). Serpentinization of abyssal peridotites from the MARK area, Mid-Atlantic Ridge: sulfur geochemistry and reaction modeling. *Geochimica et Cosmochimica Acta* **67**, 641–653.
- Bekker, A., Slack, J. F., Planavsky, N., Krapez, B., Hofmann, A., Konhauser, K. O. & Rouxel, O. J. (2010). Iron formation: the sedimentary product of a complex interplay among mantle, tectonic, oceanic, and biospheric processes. *Economic Geology* **105**, 467–508.
- Bockrath, C., Ballhaus, C. & Holzheid, A. (2004). Stabilities of laurite RuS<sub>2</sub> and monosulphide liquid solution at magmatic temperature. *Chemical Geology* **208**, 265–271.
- Brooker, R., Holloway, J. R. & Hervig, R. (1998). Reduction in piston cylinder experiments: the detection of carbon infiltration into platinum capsules. *American Mineralogist* **83**, 985–994.
- Bureau, H. & Keppler, H. (1999). Complete miscibility between silicate melts and hydrous fluids in the upper mantle: experimental evidence and geochemical implications. *Earth and Planetary Science Letters* **165**, 187–196.
- Burgisser, A. & Scaillet, B. (2007). Redox evolution of a degassing magma rising to the surface. *Nature* **445**, 194–197.
- Burgisser, A., Scaillet, B. & Harshvardhan, (2008). Chemical patterns of erupting silicic magmas and their influence on the amount of degassing during ascent. *Journal of Geophysical Research* **113**, doi:10.1029/2008JB005680.
- Burnham, C. W. (1979). The importance of volatile constituents. In: Yoder, H. S. (ed.) *The Evolution of the Igneous Rocks: Fiftieth Anniversary Perspectives*. Princeton, NJ: Princeton University Press, pp. 439–482.
- Canil, D. (2002). Vanadium in peridotites, mantle redox and tectonic environments: Archean to present. *Earth and Planetary Science Letters* **195**, 75–90.
- Carroll, M. R. & Rutherford, M. J. (1987). The stability of igneous anhydrite: Experimental results and implications for sulfur behavior in the 1982 El Chichón trachyandesite and other evolved magmas. *Journal of Petrology* **28**, 781–801.
- Carroll, M. R. & Rutherford, M. J. (1988). Sulphur speciation in hydrous experimental glasses of varying oxidation state: results from measured wavelength shifts of sulphur X-rays. *American Mineralogist* **73**, 845–849.
- Carroll, M. R. & Webster, J. D. (1994). Solubilities of sulfur, noble gases, nitrogen, chlorine, and fluorine in magmas. In: Holloway, J. R. & Carroll, M. R. (eds) *Volatiles in Magmas. Mineralogical Society of America, Reviews in Mineralogy* **30**, 231–280.
- Carroll, M. J. & Wyllie, P. J. (1989). Experimental phase relations in the system peridotite–tonalite–H<sub>2</sub>O at 15 kbar: implications for assimilation and differentiation processes at the crust–mantle boundary. *Journal of Petrology* **30**, 1351–1382.
- Catling, D. C. & Claire, M. W. (2005). How Earth's atmosphere evolved to an oxidic state: a status report. *Earth and Planetary Science Letters* **237**, 1–20.
- Cervantes, P. & Wallace, P. (2003). The role of water in subduction zone magmatism: new insights from melt inclusions in high-Mg basalts from central Mexico. *Geology* **31**, 235–238.
- Clemente, B., Scaillet, B. & Pichavant, M. (2004). The solubility of sulphur in hydrous rhyolitic melts. *Journal of Petrology* **45**, 2171–2196.
- Condie, K. C. (2008). Did the character of subduction change at the end of the Archean? Constraints from convergent-margin granitoids. *Geology* **36**, 611–614.
- Costa, F., Scaillet, B. & Pichavant, M. (2004). Petrological and experimental constraints on the pre-eruption conditions of Holocene dacite from Volcán San Pedro (36°S, Chilean Andes) and the importance of sulphur in silicic subduction-related magmas. *Journal of Petrology* **45**, 855–881.

- Defant, M. J. & Drummond, M. S. (1990). Derivation of modern arc magmas by melting of young subducted lithosphere. *Nature* **347**, 662–665.
- De Hoog, J. C. M., Taylor, B. E. & Van Bergen, M. J. (2001). Sulfur-isotope systematics of Indonesian arc basalts: Implication for the sulfur cycle in subduction zones. *Earth and Planetary Science Letters* **189**, 237–252.
- Devine, J. D., Gardner, J. E., Brach, H. P., Layne, G. D. & Rutherford, M. J. (1995). Comparison of microanalytical methods for estimation of H<sub>2</sub>O contents of silicic volcanic glasses. *American Mineralogist* **80**, 319–328.
- de Wit, M. (1998). On Archean granites, greenstones, cratons and tectonics: does the evidence demand a verdict? *Precambrian Research* **91**, 181–226.
- Ducea, M. N., McInnes, B. I. A. & Wyllie, P. J. (1999). Experimental determination of compositional dependence of hydrous silicate melts on sulfate solubility. *European Journal of Mineralogy* **11**, 33–43.
- Farquhar, J., Peters, M., Johnston, D. T., Strauss, H., Masterson, A., Wiechert, U. & Kaufman, A. (2007). Isotopic evidence for Mesoarchean anoxia and changing atmospheric sulphur chemistry. *Nature* **449**, 706–709.
- Farquhar, J., Wu, N., Canfield, D. E. & Oduro, H. (2010). Connections between sulfur cycle evolution, sulfur isotopes, sediments, and base metal sulfide deposits. *Economic Geology* **105**, 509–533.
- Gaillard, F., Pichavant, M. & Scaillet, B. (2003). Experimental determination of activities of FeO and Fe<sub>2</sub>O<sub>3</sub> components in hydrous silicic melts under oxidizing conditions. *Geochimica et Cosmochimica Acta* **67**, 4389–4409.
- Gaillard, F., Scaillet, B. & Arndt, N. T. (2011). Atmospheric oxygenation caused by a change in volcanic degassing pressure. *Nature* **478**, 229–232.
- Gomez-Tuena, A., Mori, L., Rincon-Herrera, N. E., Ortega-Gutierrez, F., Sole, J. & Iriondo, A. (2008). The origin of a primitive trondhjemitic from the Trans Mexican Volcanic Belt and its implication for the construction of a modern continental arc. *Geology* **36**, 471–475.
- Habicht, K. S., Gade, M., Thamdrup, B., Berg, P. & Canfield, D. E. (2002). Calibration of sulfate levels in the Archean ocean. *Science* **298**, 2372–2374.
- Hall, L. J., Brodie, J., Wood, B. J. & Carroll, M. R. (2004). Iron and water losses from hydrous basalts contained in Au80Pd20 capsules at high pressure and temperature. *Mineralogical Magazine* **68**, 75–81.
- Hermann, J. & Spandler, C. J. (2008). Sediment melts at sub-arc depths: an experimental study. *Journal of Petrology* **49**, 717–740.
- Hermann, J., Spandler, C. J., Hack, A. & Korsakov, A. V. (2006). Aqueous fluids and hydrous melts in high-pressure and ultra-high pressure rocks: Implications for element transfer in subduction zones. *Lithos* **92**, 399–417.
- Holland, H. D. (2002). Volcanic gases, black smokers, and the Great Oxidation Event. *Geochimica et Cosmochimica Acta* **66**, 3811–3826.
- Holland, H. D. (2009). Why the atmosphere became oxygenated: A proposal. *Geochimica et Cosmochimica Acta* **73**, 5241–5255.
- Holloway, J. R., Pan, V. & Gudmunsson, G. (1992). High pressure fluid absent melting experiments in the presence of graphite: oxygen fugacity, ferric/ferrous ratio and dissolved CO<sub>2</sub>. *European Journal of Mineralogy* **4**, 105–114.
- Holzeid, A. & Grove, T. L. (2002). Sulfur saturation limits in silicate melts and their implications for core formation scenarios for terrestrial planets. *American Mineralogist* **87**, 227–237.
- Hopkins, M., Harrison, T. M. & Manning, C. M. (2008). Low heat flow inferred from >4 Gyr zircons suggests Hadean plate boundary interactions. *Nature* **451**, 493–496.
- Huston, D. L., Pehrsson, S., Eglinton, B. M. & Zaw, K. (2010). The geology and metallogeny of volcanic-hosted deposits: variations through geologic time and with tectonic setting. *Economic Geology* **105**, 571–591.
- Jambon, A. (1994). Earth degassing and large scale geochemical cycling of volatile elements. In: Carroll, M. R. & Holloway, J. R. (eds) *Volatiles in Magmas. Rev. Mineral* **30**, 479–509.
- Johnson, E. R., Wallace, P. J., Granados, H. D., Manea, V. C., Kent, A. R., Bindeman, I. N. & Donegan, C. S. (2009). Subduction related Volatile Recycling and Magma Generation beneath Central Mexico: Insights from Melt Inclusions, Oxygen Isotopes and Geodynamic Models. *Journal of Petrology* **50**, 1729–1764.
- Johnson, M. C. & Plank, T. (1999). Dehydration and melting experiments constrain the fate of subducted sediments. *Geochemistry, Geophysics, Geosystems* **1**, 1007, doi:10.1029/1999GC000014.
- Jugo, P. J. & Luth, R. W. (2005). Experimental data on the speciation of sulfur as a function of oxygen fugacity in basaltic melts. *Geochimica et Cosmochimica Acta* **69**, 497–503.
- Jugo, P. J., Luth, R. W. & Richards, J. P. (2005). An experimental study of the sulfur content in basaltic melts saturated with immiscible sulfide or sulfate liquids at 1300°C and 10 GPa. *Journal of Petrology* **46**, 783–798.
- Jugo, P. J., Wilke, M. & Botcharnikov, R. E. (2010). Sulfur K-edge XANES analysis of natural and synthetic basaltic glasses: Implications for S speciation and S content as function of oxygen fugacity. *Geochimica et Cosmochimica Acta* **74**, 5926–5938.
- Kelemen, P. B. (1995). Genesis of high Mg# andesites and the continental crust. *Contributions to Mineralogy and Petrology* **120**, 1–19.
- Kelemen, P. B., Rilling, J. L., Parmentier, E. M., Mehl, L. & Hacker, B. R. (2003). Thermal structure due to solid-state flow in the mantle wedge beneath arcs. In: Eiler, J. (ed.) *Inside the Subduction Factory. Geophysical Monograph, American Geophysical Union* **138**, 293–311.
- Kepler, H. (1999). Experimental evidence for the source of excess sulfur in explosive volcanic eruptions. *Science* **284**, 1652–1654.
- Kessel, R., Schmidt, M. W., Ulmer, P. & Pettke, T. (2005a). Trace element signature of subduction-zone fluids, melts and supercritical liquids at 120–180 km depth. *Nature* **437**, 724–727.
- Kessel, R., Ulmer, P., Pettke, P., Schmidt, M. W. & Thompson, A. B. (2005b). Experimental determination of phase relations and second critical end point in K-free eclogite–H<sub>2</sub>O at 4–5 GPa and 700–1400°C. *Earth and Planetary Science Letters* **237**, 873–892.
- Klimm, K. & Botcharnikov, R. E. (2010). The determination of sulfate and sulfide species in hydrous silicate glasses using Raman spectroscopy. *American Mineralogist* **95**, 1574–1579.
- Klimm, K., Blundy, J. & Green, T. H. (2008). Trace element partitioning and accessory phase saturation during H<sub>2</sub>O-saturated melting of basalt with implications for subduction zone chemical fluxes. *Journal of Petrology* **49**, 523–553.
- Kress, V. C. (1997). Thermochemistry of sulfide liquids. I. The system O–S–Fe at 1 bar. *Contributions to Mineralogy and Petrology* **127**, 176–186.
- Kress, V. C. & Carmichael, I. S. E. (1991). The compressibility of silicate liquids containing Fe<sub>2</sub>O<sub>3</sub> and the effect of composition, temperature, oxygen fugacity and pressure on their redox states. *Contributions to Mineralogy and Petrology* **108**, 82–92.
- Kump, L. R. & Barley, M. E. (2007). Increased subaerial volcanism and the rise of atmospheric oxygen 2.5 billion years ago. *Nature* **448**, 1033–1036.
- Leake, B. E., Wooley, A. R., Arps, C. E. S., Birch, W. D., Gilbert, M. C., Grice, J. D., Hawthorne, F. C., Kato, A., Kish, H. J., Krivovichef, V. G., Linthout, K., Laird, J., Mandarino, J., Maresch, W. V., Nickel, E. H., Rock, N. M. S., Schumacher, J. C., Smith, D. C., Stephenson, N. C. N., Ungaretti, L.,

- Whittaker, E. J. W. & Youzhi, G. (1997). Nomenclature of amphiboles. Report of the Subcommittee on Amphiboles of the International Mineralogical Association Commission on New Minerals and Mineral names. *European Journal of Mineralogy* **9**, 623–651.
- Li, Z. X. A. & Lee, C. T. A. (2005). The constancy of upper mantle  $f_{\text{O}_2}$  through time inferred from V/Sc ratios in basalts. *Earth and Planetary Science Letters* **228**, 483–493.
- Liu, Y., Samaha, N. T. & Baker, D. B. (2007). Sulfur concentration at sulfide saturation (SCSS) in magmatic silicate melts. *Geochimica et Cosmochimica Acta* **71**, 1783–1799.
- Luhr, J. F. (1990). Experimental phase relations of water- and sulphur-saturated arc magmas and the 1982 eruptions of El Chichon volcano. *Journal of Petrology* **31**, 1071–1114.
- Lyons, T. W. & Gill, B. C. (2010). Ancient sulfur cycling and oxygenation of the early biosphere. *Elements* **6**, 93–99.
- Martel, C., Pichavant, M., Bourdier, J. L., Traineau, H., Holtz, F. & Scaillet, B. (1998). Magma storage conditions and control of eruption regime in silicic volcanoes: experimental evidence from Mt. Pelée. *Earth and Planetary Science Letters* **156**, 89–99.
- Martin, H. (2005). Genesis and evolution of the primitive Earth continental crust. In: Gargaud, M., Barbier, B., Martin, H. & Reisse, J. (eds) *Lectures in Astrobiology I*. Berlin: Springer, pp. 113–163.
- Mavrogenes, J. A. & O'Neill, H. S. C. (1999). The relative effects of pressure, temperature and oxygen fugacity on the solubility of sulfide in mafic magmas. *Geochimica et Cosmochimica Acta* **63**, 1173–1180.
- Métrich, N. & Clocchiatti, R. (1996). Sulfur abundance and its speciation in oxidized alkaline melts. *Geochimica et Cosmochimica Acta* **60**, 4151–4160.
- Métrich, N., Schiano, P., Clocchiatti, R. & Maury, R. C. (1999). Transfer of sulfur in subduction zones settings: an example of Batan island (Luzon volcanic arc, Philippines). *Earth and Planetary Science Letters* **167**, 1–14.
- Moretti, R. & Baker, D. R. (2008). Modelling the interplay of  $f_{\text{O}_2}$  and  $f_{\text{S}_2}$  along the FeS–silicate melt equilibrium. *Chemical Geology* **256**, 286–298.
- Moune, S., Holtz, F. & Botcharnikov, R. (2009). Sulphur solubility in andesitic to basaltic melts: implications for Hekla volcano. *Contributions to Mineralogy and Petrology* **157**, 691–707.
- Nair, R. & Chacko, T. (2008). Role of oceanic plateaus in the initiation of subduction and origin of continental crust. *Geology* **36**, 583–586, doi:10.1130/G24773A.1.
- Newton, R. C. & Manning, C. E. (2005). Solubility of anhydrite,  $\text{CaSO}_4$ , in  $\text{NaCl-H}_2\text{O}$  solutions at high pressures and temperatures: applications to fluid–rock interaction. *Journal of Petrology* **46**, 701–716.
- Nichols, G. T., Wyllie, P. J. & Stern, C. R. (1994). Subduction zone melting of pelagic sediments constrained by melting experiments. *Nature* **371**, 785–788.
- O'Neill, H. S. C. & Mavrogenes, J. A. (2002). The sulfide capacity and the sulfur content at sulfide saturation of silicate melts at 1400°C and 1 bar. *Journal of Petrology* **43**, 1049–1087.
- Parat, F., Holtz, F. & Feig, S. (2008). Pre-eruptive Conditions of the Huerto Andesite (Fish Canyon System, San Juan Volcanic Field, Colorado): Influence of Volatiles (C-O-H-S) on Phase Equilibria and Mineral Composition. *Journal of Petrology* **49**, 911–935.
- Patiño Douce, A. & Beard, J. (1994).  $\text{H}_2\text{O}$  loss from hydrous melts during fluid-absent piston cylinder experiments. *American Mineralogist* **79**, 585–588.
- Pichavant, M., Mysen, B. O. & Macdonald, R. (2002). Source and  $\text{H}_2\text{O}$  content of high-MgO magmas in island arc settings: An experimental study of a primitive calc-alkaline basalt from St. Vincent, Lesser Antilles arc. *Geochimica et Cosmochimica Acta* **66**, 2193–2209.
- Plank, T., Cooper, L. B. & Manning, C. E. (2009). Emerging geothermometers for estimating slab surface temperatures. *Nature Geoscience* **2**, 611–615, doi:10.1038/ngeo614.
- Popp, R. K., Gilbert, M. C. & Craig, J. R. (1977). Stability of Fe–Mg amphiboles with respect to sulfur fugacity. *American Mineralogist* **62**, 13–30.
- Prouteau, G., Scaillet, B., Pichavant, M. & Maury, R. (2001). Evidence for mantle metasomatism by hydrous silicic melts derived from subducted oceanic crust. *Nature* **410**, 197–200.
- Rapp, R. P. & Watson, E. B. (1995). Dehydration melting of metabasalt at 8–32 kbar: implications for continental growth and crust–mantle recycling. *Journal of Petrology* **36**, 891–931.
- Rapp, R. P., Shimizu, N., Norman, M. D. & Applegate, G. S. (1999). Reaction between slab-derived melts and peridotite in the mantle wedge: experimental constraints at 3–8 GPa. *Chemical Geology* **160**, 335–356.
- Ratajeski, K. & Sisson, T. W. (1999). Loss of iron to gold capsules in rock-melting experiments. *American Mineralogist* **84**, 1521–1527.
- Robock, A. (2000). Volcanic eruptions and climate. *Reviews in Geophysics* **38**, 191–219.
- Rosenbaum, J. M. & Slagel, M. M. (1995). C–O–H speciation in piston cylinder experiments. *American Mineralogist* **80**, 109–114.
- Scaillet, B. & Evans, B. W. (1999). The June 15, 1991 eruption of Mount Pinatubo. I. Phase equilibria and pre-eruption  $P$ – $T$ – $f_{\text{O}_2}$ – $f_{\text{H}_2\text{O}}$  conditions of the dacite magma. *Journal of Petrology* **40**, 381–411.
- Scaillet, B. & Macdonald, R. (2006). Experimental and thermodynamic constraints on the sulphur yield of peralkaline and metaluminous silicic flood eruptions. *Journal of Petrology* **47**, 1413–1437.
- Scaillet, B., Pichavant, M., Roux, J., Humbert, G. & Lefevre, A. (1992). Improvements of the Shaw membrane technique for measurement and control of  $f_{\text{H}_2}$  at high temperatures and pressures. *American Mineralogist* **77**, 647–655.
- Scaillet, B., Pichavant, M. & Roux, J. (1995). Experimental crystallization of leucogranite magmas. *Journal of Petrology* **36**, 663–705.
- Scaillet, B., Clemente, B., Evans, B. W. & Pichavant, M. (1998). Redox control of sulfur degassing in silicic magmas. *Journal of Geophysical Research* **103**, 23937–23949.
- Scaillet, B., Luhr, J. F. & Carroll, M. C. (2003). Petrological and volcanological constraints on volcanic sulfur emissions to the atmosphere. In: Robock, A. & Oppenheimer, C. (eds) *Volcanism and the Earth's Atmosphere*. *Geophysical Monograph, American Geophysical Union* **139**, 11–40.
- Schiano, P., Clocchiatti, R., Shimizu, N., Maury, R. C., Jochum, K. P. & Hofmann, A. W. (1995). Hydrous, silica-rich melts in the sub-arc mantle and their relationship with erupted arc lavas. *Nature* **377**, 595–600.
- Schmidt, M. W. (1996). Experimental constraints on recycling of potassium from subducted oceanic crust. *Science* **272**, 1927–1930.
- Schmidt, M. W. & Poli, S. (1998). Experimentally based water budgets for dehydrating slabs and consequences for arc magma generation. *Earth and Planetary Science Letters* **163**, 361–379.
- Schmidt, M. W., Vielzeuf, D. & Auzanneau, E. (2004). Melting and dissolution of subducting crust at high pressures: the key role of white mica. *Earth and Planetary Science Letters* **228**, 65–84.
- Sekine, T. & Wyllie, P. J. (1983). Experimental simulation of mantle hybridization in subduction zones. *Journal of Geology* **91**, 511–528.
- Sen, C. & Dunn, T. (1995). Experimental modal metasomatism of a spinel lherzolite and the production of amphibole-bearing peridotite. *Contributions to Mineralogy and Petrology* **119**, 422–432.

- Smithies, R. H. (2000). The Archean tonalite–trondhjemite–granodiorite (TTG) series is not an analogue of Cenozoic adakite. *Earth and Planetary Science Letters* **182**, 115–125.
- Spandler, C., Yaxley, G., Green, D. H. & Scott, D. (2010). Experimental phase and melting relations of metapelite in the upper mantle: implications for the petrogenesis of intraplate magmas. *Contributions to Mineralogy and Petrology* **160**, 569–589, doi:10.1007/s00410-010-094-2.
- Thomsen, T. B. & Schmidt, M. W. (2008). Melting of carbonated pelites at 2.5–5.0 GPa, silicate–carbonatite liquid immiscibility, and potassium–carbon metasomatism of the mantle. *Earth Planetary Science Letters* **267**, 17–31.
- Tomkins, A. G. (2010). Windows of metamorphic sulfur liberation in the crust: implications for gold deposit genesis. *Geochimica et Cosmochimica Acta* **74**, 3246–3259.
- Toulmin, P. I. & Barton, P. B. J. (1964). A thermodynamic study of pyrite and pyrrhotite. *Geochimica et Cosmochimica Acta* **28**, 641–671.
- Truckenbrodt, J., Ziegenbein, D. & Johannes, W. (1997). Redox conditions in piston cylinder apparatus: the different behavior of boron nitride and unfired pyrophyllite assemblies. *American Mineralogist* **82**, 337–344.
- Tso, J. L., Gilbert, M. L. & Craig, J. R. (1979). Sulfidation of synthetic biotites. *American Mineralogist* **64**, 304–316.
- Tsuno, K. & Dasgupta, R. (2011). Melting phase relation of nominally anhydrous, carbonated pelitic-eclogite at 2.5–3.0 GPa and deep cycling of sedimentary carbon. *Contributions to Mineralogy and Petrology* **161**, 743–763.
- Ulmer, P. & Luth, R. W. (1991). The graphite–COH fluid equilibrium in  $P, T, fO_2$  space. An experimental determination to 30 kbar and 1600°C. *Contributions to Mineralogy and Petrology* **106**, 265–272.
- Ulmer, P. & Trommsdorff, V. (1995). Serpentine stability to mantle depth and subduction related magmatism. *Science* **268**, 858–861.
- van der Laan, S. R. & Wyllie, P. J. (1992). Constraints on Archean trondhjemite genesis from hydrous crystallisation experiments on Nùk gneiss at 10–17 kbar. *Journal of Geology* **100**, 57–68.
- van Keken, P. E., Kiefer, B. & Peacock, S. (2002). High-resolution models of subduction zones: implications for mineral dehydration reactions and the transport of water into the deep mantle. *Geochemistry, Geophysics, Geosystems* **3(10)**, 1056, doi:10.1029/2001GC000256.
- Wallace, P. J. (2005). Volatiles in subduction zone magmas: concentrations and fluxes based on melt inclusion and volcanic gas data. *Journal of Volcanology and Geothermal Research* **140**, 217–240.
- Wallace, P. J. & Carmichael, I. S. E. (1992). Sulfur in basaltic magmas. *Geochimica et Cosmochimica Acta* **56**, 1683–1874.
- Webster, J. D., Holloway, J. R. & Hervig, R. L. (1987). Phase equilibria of a Be, U and F-enriched vitrophyre from Spor Mountain, Utah. *Geochimica et Cosmochimica Acta* **51**, 389–402.
- Wendlandt, R. F. (1982). Sulfide saturation of basalt and andesite melts at high pressures and temperatures. *American Mineralogist* **67**, 877–885.
- Whitney, J. A. (1972). The effect of reduced  $H_2O$  fugacity on the buffering of oxygen fugacity in hydrothermal experiments. *American Mineralogist* **57**, 1902–1908.
- Whitney, J. A. (1984). Fugacities of sulphurous gases in pyrrhotite bearing silicic magmas. *American Mineralogist* **69**, 69–78.
- Winther, K. T. (1996). An experimental based model for the origin of tonalitic and trondhjemitic melts. *Chemical Geology* **127**, 43–59.
- Wykes, J. L. & Mavrogenes, J. A. (2005). Hydrous sulfide melting: experimental evidence for the solubility of  $H_2O$  in sulfide melts. *Economic Geology* **100**, 157–164.
- Zhang, Y. (1999).  $H_2O$  in rhyolitic glasses and melts: measurement, speciation, solubility, and diffusion. *Reviews of Geophysics* **37**, 493–516.